Palaeomagnetic constraints from granodioritic plutons (Jiaodong Peninsula): New insights on Late Mesozoic continental extension in eastern Asia.

Nicolas Charles, Yan Chen, Romain Augier, Charles Gumiaux, Wei Lin, Michel Faure, Patrick Monié, Flavien Choulet, Fuyuan Wu, Rixiang Zhu, et al.

Palaeomagnetic constraints from granodioritic plutons (Jiaodong Peninsula): New insights on Late Mesozoic continental extension in eastern Asia.

Nicolas CHARLES[1,*], Yan CHEN[1], Romain AUGIER[1], Charles GUMIAUX[1], Wei LIN[2], Michel FAURE[1], Patrick MONIÉ[3], Flavien CHOULET[1], Fuyuan WU[2], Rixiang ZHU[2], Qingchen WANG[2].

1. Institut des Sciences de la Terre d'Orléans (ISTO)
   Université d'Orléans-CNRS/INSU (UMR6113)
   1A, rue de la Férollerie
   45071 Orléans cedex 2
   France
2. Institute of Geology and Geophysics, Chinese Academy of Sciences
   Beituchengxi road 19
   100021 Beijing
   China
3. Géosciences Montpellier
   Université Montpellier 2-CNRS (UMR5243)
   Place E. Bataillon
   34095 Montpellier cedex 5
   France

*Corresponding author: nicolas.charles@univ-orleans.fr; (nicolas.charlesmoreau@yahoo.fr)

Abstract

Mechanism and kinematics of the Late Mesozoic continental extension event of eastern Asia are still debated. In order to better constrain its evolution, two granodioritic plutons of the Jiaodong Peninsula have been chosen as targets for a time-constrained palaeomagnetic study. Indeed, plutons are devoid of visible deformation, did not experience rotation along horizontal axis and are precisely dated by U/Pb and $^{40}Ar/^{39}Ar$ methods. Multidomain (MD) magnetite has been identified as the principal magnetic remanent carrier. The interpolation of existing and new U/Pb and $^{40}Ar/^{39}Ar$ ages revealed that characteristic remanent magnetisation was acquired in a narrow range of 116 ± 2 Ma. Twenty out of 27 sites present stable magnetic directions calculated from high-temperature or high-coercive components. The observations of the solo normal magnetic polarity for this palaeomagnetic collection and of the magnetic remanent age consistent with the Cretaceous Normal Superchron (CNS) argue that the characteristic magnetic remanence may be considered as primary. Detailed field observations of the intrusive relationship between the plutons and country rocks and Anisotropy of Magnetic Susceptibility (AMS) study reveal the absence of the subsequent deformation of plutons, or rigid rotation of plutons along a horizontal axis. Two palaeomagnetic poles have been therefore calculated from these plutons. Among 12 out 15 Cretaceous palaeomagnetic poles, including the two new poles provided by this study, from the Jiaodong Peninsula and on both sides of Tan-Lu and Muping-Jimo faults are statistically consistent. As a result, the Jiaodong Peninsula behaved as a rigid block as internal deformation appears negligible. The remaining three derived poles are probably due to the secular variation or/and the vicinity of fault zones near of the palaeomagnetic sampling site. Thus, they can not be applied to the peninsula-scaled tectonics. Comparison of these time-constrained Cretaceous palaeomagnetic results of the Jiaodong Peninsula with those of North China Block (NCB) indicate that the Jiaodong Peninsula was rigidly attached to NCB since,

at least, the Cretaceous as residual difference is clearly insignificant with respect to the error brackets. These new palaeomagnetic results confirm that the relative clockwise (CW) rotation of Eastern Liaoning-Korea Block (ELKB) with respect to NCB does not affect the Jiaodong Peninsula as a rigid block, nevertheless, some tectonic structures have been reactivated since Cenozoic and local rotations could be produced. This palaeomagnetic study reveals that the Late Mesozoic extension in Eastern Asia is heterogeneously expressed in time and space. The complete understanding of the mechanism(s) of this extensional event needs further multidisciplinary investigations.

Key-words: Eastern China, Late Mesozoic extension, palaeomagnetism, granitic pluton, magnetic remanent age, Cretaceous, Shandong Peninsula.

1. Introduction

After a succession of Palaeozoic orogenies and a relative tectonic quietude (e.g., Kusky et al., 2007), Eastern Asia has experienced a major extensional event and lithospheric thinning during Late Mesozoic and Cenozoic times that extend from South China to Lake Baikal south-northwardly and from the Japanese Islands to Gobi desert east-westwardly (e.g., Gilder et al., 1991; Menzies et al., 1993; Davis et al., 1996; Griffin et al., 1998; Ren et al., 2002; Lin et al., 2003; Meng, 2003; Lin and Wang, 2006; Zhai et al., 2007; Daoudene et al., 2009; Chen, 2010). Numerous geological observations argue for the importance of this major extensional event, including: (1) formation of intracontinental extensional sedimentary basins (e.g., Liu, 1986; Ma and Wu, 1987; Ren et al., 2002), (2) emplacement of widespread volcanism and plutonism (Wu et al., 2005a, b, 2007) and more importantly (3) exhumation of Metamorphic Core Complexes (MCC; Davis et al., 1996; Darby et al., 2004; Liu et al., 2005; Lin et al., 2008; Charles et al., 2011). It is noteworthy that most of these features developed

during the Late Jurassic-Early Cretaceous (e.g., Ren et al., 2002; Liu et al., 2005; Wu et al., 2005a; Wang et al., 2006; Lin et al., 2008). Various models proposed to account for the geodynamical causes for this major extensional event are still highly debated (e.g., Meng, 2003; Lin and Wang, 2006; Zhai et al., 2007): (1) back-arc extension induced from Palaeo-Pacific plate subduction (e.g., Watson et al., 1987; Li, 2000; Zhou and Li, 2000; Ren et al., 2002), (2) post-orogenic collapse (Meng, 2003), (3) lithospheric delamination (Lin and Wang, 2006), or (4) mantle plume (Okada, 1999).

The Late Mesozoic to Cenozoic extensional event affected eastern Asia composed of a set of continental blocks amalgamated during previous orogenies (e.g., Mattauer et al., 1985; Kusky et al., 2007). The knowledge of kinematic histories of these blocks during Late Mesozoic times can provide essential informations to better understand relations between rigid blocks movement of and development of major extensional crustal structures. In fact, according to palaeomagnetic and structural studies, Lin et al. (2003) and Liu et al. (2005) have proposed that clockwise (CW) rotation of the Eastern Liaoning-Korean block (ELKB) with respect to the North China Block (NCB) was accommodated by the exhumation of South Liaodong and Yiwulüshan MCCs and the opening of Songliao-Xialiaohe basin (see Fig. 1 in Lin et al., 2003). Moreover, the Euler pole of this CW rotation is located in the southern end of Bohai bay (Lin et al., 2003). Such a CW rotation is also invoked by Huang et al. (2007) for the easternmost and southeastern parts of the Jiaodong Peninsula (Shandong Province, NE China) to the south of the ELKB and the Bohai bay, since Early Cretaceous. As a result, Huang et al. (2007) assume that the Jiaodong Peninsula cannot be considered as a rigid part of the NCB. However, an other palaeomagnetic study carried out in the peninsula showed that the northern part of the Jiaodong did not experience any rotation nor latitudinal displacement since Cretaceous times with respect to NCB (Gilder et al., 1999). These discrepancies have major consequences on the understanding of the mechanism of the Mesozoic extension in the

eastern Asia and thus, need to be clarified. The aim of the present paper is to better palaeomagnetically constrain the kinematics of the Jiaodong Peninsula with well-dated ferromagnetic granodioritic plutons (i.e. the Weideshan and Haiyang massifs; Fig. 1 and Table 1). This palaeomagnetic study has been carried out with careful structural and AMS analyses of both plutons and country rocks. New palaeomagnetic and time constraints are thus provided to better understand the Late Mesozoic extension of Eastern Asia.

2. Geological background

2.1. Jiaodong Peninsula

The Jiaodong Peninsula, in Shandong Province (NE China), is located along the southeastern margin of the North China Block (NCB; Fig. 1a). This area is delimited to the west by the NNE-trending crustal-scale Tancheng-Lujiang (or Tan-Lu) fault (Fig. 1a), and to the south by the Sulu ultrahigh-pressure metamorphic belt which was tectonically active during Triassic times (e.g., Faure et al., 2001, 2003). To the northwest of the Jiaodong Peninsula, Precambrian basement rocks are uncomformably covered by Mesozoic to Cenozoic sedimentary and volcanic series (Fig. 1b; e.g., SBGMR, 1991). Precambrian basement rocks consist of (1) Late Archaean gneisses, granulites, amphibolites and micaschists (Jiaodong Group), unconformably overlain by (2) Palaeoproterozoic multimodal volcanic and sedimentary rocks metamorphosed to amphibolite-granulite facies (Jinshan and Fengzishan Groups) and (3) Neoproterozoic (Sinian) metasedimentary rocks (Penglai Group).

Mesozoic rocks are mainly composed of Cretaceous volcano-sedimentary rocks present in extensional intracontinental sedimentary basins (e.g., the Jiaolai basin). Cretaceous stratigraphic series consist into three volcano-sedimentary groups (Laiyang Group dated from ~138 to 126 Ma, Qingshan Group dated from ~126 to 100 Ma, and Wangshi Group dated to the Late Cretaceous K_2; Yu, 1990; Liu et al., 1994; Qiu et al., 2001; Song and Wang, 2003;

Yan et al., 2003; Zhang et al., 2003). These latter series are mainly exposed in the Jiaolai extensional basin (Zhang et al., 2003) and were already sampled for palaeomagnetic studies (Gilder et al., 1999; Huang et al., 2007). Both Precambrian basement rocks and most sedimentary series are intruded by large volume of Late Jurassic to Early Cretaceous plutonic rocks (Fig. 1b). They are divided into two well-defined temporal suites (Sang, 1984; SBGMR, 1991; Wang et al., 1998): (1) Late Jurassic granitoids derived from a crustal source (partial melting of upper crustal rocks) (e.g., Luanjiahe, Kunyushan, Wendeng massifs) and (2) Early Cretaceous granitoids derived from partial-melting of lower crustal levels with a significant contribution of upper mantle (e.g., Aishan, Haiyang, Weideshan, Sanfoshan massifs). These granitic rocks are involved in different geological structures linked to a Late Mesozoic NW-SE extensional setting (Charles, 2010; Charles et al., 2011). Indeed, the Late Jurassic Linglong monzogranite is associated with migmatites, and both of them constitute the Linglong Metamorphic Core Complex (MCC) exhumed below the Linglong detachment fault (LDF) before 134 Ma (Fig. 1b; Charles, 2010). Besides, the Early Cretaceous Guojialing granodiorite is a synkinematic pluton emplaced below the Guojialing shear zone (GSZ) at around 124 Ma (Fig. 1b; Charles, 2010). Granitic rocks also occur as unstrained intrusive plutons into the upper crust and the sedimentary cover (e.g., Late Jurassic Luanjiahe pluton, Early Cretaceous Haiyang and Weideshan plutons). Emplacement and cooling ages of these granitic rocks are particularly well constrained in the region (e.g., Wang et al., 1998) and provide more accurate time-constrained samples for palaeomagnetic aims than surrounding country sedimentary rocks.

2.2. Weideshan and Haiyang granitic plutons

Both the Weideshan and Haiyang plutons are composed of pinkish-reddish granodiorite with a high proportion of pink K-feldspar, and show porphyritic textures with

large microcline megacrysts and medium to coarse-grained groundmass (SBGMR, 1991; Yang and Lü, 1996). Graphic and miarolitic textures with quartz crystals aggregates in the miarolitic cavities are commonly observed (e.g., SBGMR, 1991; Wu and Lin, 1991; Zhou and Lü, 2000). The main accessory minerals include magnetite, apatite, zircon and titanite. Geochemical analyses of these plutons yielded $^{87}Sr/^{86}Sr$ ratios ranging from 0.7050 to 0.7076 (Li and Yang, 1993) highlighting a significant upper mantle contribution (Song and Yan, 2000).

The Weideshan massif is an elliptic granodioritic pluton (~520 km²) located in the easternmost part of Jiaodong Peninsula (Figs. 1b and 2a), to the north of Rongcheng city and to the east of the Muping-Jimo fault (Fig. 1b). U/Pb analyses on zircon yielded an age of 118 ± 2 Ma (Zhang et al., 2007). In the field, granodioritic rocks appear devoid of macroscopic deformation and present isotropic textures. Structural investigations along its contact with the country rocks show clear intrusive relationships either devoid of subsequent penetrative deformation or brittle faulting. Anisotropy of magnetic susceptibility (AMS) study has been carried out to access to planar and linear structural fabrics and showed that magnetic foliation trajectories design concentric patterns (Charles, 2010; Fig. 2a). Moreover, magnetic foliations are mainly subhorizontal to gently-dipping at the pluton-scale (Fig. 2c). Magnetic lineations are scattered and present sub-horizontal plunges (Fig. 2c). Corrected anisotropy degree P_J (Jelinek, 1981) shows low values (mean value of P_J for the pluton = 1.123) which denotes that granitic rocks of the Weideshan pluton did not experience significant deformation since the AMS acquisition (Fig. 2e; Charles, 2010). Gravity data point to the existence of a main feeder zone located below the pluton centre where the Bouguer anomaly value is the lowest (i.e. -16 mGal; Ma, 1997). Structural and geophysical data imply that the pluton did not experience any rotation along a horizontal axis with respect to the country rocks.

The Haiyang granodioritic pluton (~480 km²) is located in the southwest part of Jiaodong Peninsula, close to Rushan and Haiyang cities, and east of the Muping-Jimo fault (Figs. 1b and 2b). Available Jurassic Rb-Sr ages available for this pluton (156-147 Ma; SBGMR, 1991) do not make geological sense since these granodioritic rocks are clearly intrusive into Early Cretaceous sediments (i.e. Laiyang Group) leading to consider an intrusion age younger than ~126 Ma (consistent age of volcanic rocks of the Laiyang Group; Yu, 1990; Liu et al., 1994). This age discrepancy motivated the geochronological study of these rocks with both U/Pb and $^{40}Ar/^{39}Ar$ methods on zircon and biotite to recognise emplacement and cooling ages of the Haiyang pluton. Thanks to good outcrop exposures, intrusive contact with Early Cretaceous layers has been observed (Figs. 1b and 2b). There, horizontal to gently dipping strata indicates that sedimentary cover has not been significantly tilted during and more importantly after the emplacement of the pluton. Intrusion induced a metamorphic aureole with development of hornfels in the country rocks. Neither ductile nor brittle deformation has been observed along the contact between pluton and country rocks. AMS investigations show concentric pattern for magnetic foliation trajectories accompanied with subhorizontal magnetic lineations and foliations (Charles, 2010; Figs. 2b and 2d). Low values of the corrected anisotropy degree P_J (mean value of P_J for the pluton = 1.080) imply that granitic rocks of the Haiyang pluton did not experience significative post-solidus strain since the AMS acquisition (Fig. 2e; Charles, 2010). Bouguer anomaly values involve a main feeder zone centered on the pluton cartographic outline (i.e. -14 mGal; Ma, 1997). Similarly to the Weideshan pluton, structural and geophysical evidences show that the Haiyang pluton has not undergone any rotation along a horizontal axis.

3. Geochronological study of the Haiyang pluton

3.1. Aim, sampling and sample description

Palaeomagnetism relies on the study of magnetic remanence involved by ferromagnetic minerals present in rocks. Such minerals record Earth field directions when rocks attempt a specific temperature below which magnetic field is "fossilised". Knowledge of both pluton emplacement age and subsequent cooling history is thus essential to determine accurately the age of remanence. Up to now, not any reliable time-constraint is available for the Haiyang pluton. Available Rb-Sr ages, ranging from 156 to 147 Ma are clearly in conflict with the intrusive character of the pluton into Early Cretaceous sedimentary layers of the Jiaolai basin (SBGMR, 1991) and thus, cannot be used to constrain the emplacement age of the Haiyang pluton. Granodiorite samples were consequently collected to perform new U/Pb and $^{40}Ar/^{39}Ar$ analyses on zircon and biotite. Samples 07-056 and KH283 (see location in Fig. 2b) were picked from operating quarries to avoid any mineral alteration, especially for biotite. More details on U/Pb and $^{40}Ar/^{39}Ar$ analytical methods are given in Appendix A and B respectively. Samples 07-056 and KH283 are a porphyritic granodiorite essentially composed of quartz, large pink K-feldspar, plagioclase, biotite and amphibole. The rock does not show any deformation either on outcrop or in thin-section.

3.2. Results

3.2.1 U/Pb analyses on zircons

Analysed zircons display a homogeneous population of >100µm sized grains in length (Fig. 3a). According to the typology proposed by Pupin (1980), zircons with a rather prismatic habit are characteristic of high temperatures (between 750-900°C). After data reduction (GLITTER software; Jackson et al., 2004) and common Pb corrections (Andersen, 2002), isotopic ratios were plotted into an inverted concordia diagram (Tera and Wasserburg,

1972). Eight analyses (Table 2) yielded a lower intercept age of 117.8 ± 2.7 Ma (Fig. 3b) interpreted as the cooling below 800°C (i.e. Spear, 1993; Cherniak and Watson, 2000) shortly after granodiorite crystallisation. More details on isotopic measurements are given in Table 2.

3.2.2. $^{40}Ar/^{39}Ar$ analyses on biotite

Chemical compositions of biotite were obtained by using the CAMECA SX50 electron microprobe (BRGM-ISTO Orléans), results are presented in Figure 3c. Biotites chemistry show very slight compositional variability with K_2O wt% = 9.14-9.90 and Fe/(Fe+Mg) ratios ranging from 0.38 to 0.41. $^{40}Ar/^{39}Ar$ analyses were carried out following a conventional procedure for 15 increasing temperature steps (Fig. 3d and Table 3). Age spectrum, given on figure Fig. 3d yielded a plateau age segment for 78% of the gas released at 115.4 ± 1.2 Ma, consistent with both total fusion age (TFA, 115.5 ± 0.3 Ma) and isochron age (115.7 ± 1.2 Ma). This age is interpreted as the time elapsed since the rock sample cooled below the closure temperature of the K/Ar isotopic system for biotite settled at 300 ± 30°C (Villa, 1998).

4. Palaeomagnetic study on granodioritic plutons of Jiaodong Peninsula

With respects to their bulk chemistry (SBGMR, 1991) the Weideshan and Haiyang plutons are characterised by the relative abundance of ferromagnetic minerals, such as magnetite. Their unstrained character together with their intrusive relationships into undeformed Lower Cretaceous strata, make them highly suitable for accurate palaeomagnetic study. Furthermore, magnetic remanent ages accurately constrained by a critical compilation of geochronological data completed by new acquired time constraints, allow to obtain new kinematic constraints of Jiaodong Peninsula since Cretaceous times.

4.1. Palaeomagnetic sampling

Palaeomagnetic samples were collected from 27 sites, 13 from the Weideshan pluton and 14 sites from the Haiyang pluton (Table 1 and Figs. 2a and 2b). These sites have been chosen based on their geographic location so as to obtain a representative spatial distribution for each pluton (Figs. 2a and 2b). Sampling was carried out with a portable gasoline drill and the cores were oriented with magnetic and solar compasses, when it was possible. The average difference between magnetic and solar declinations is about -6.5° ± 2.7° and -6.8° ± 2.5° for the Weideshan and Haiyang plutons, respectively. As a result, an azimuth measurement has been corrected to cores that have been only magnetically oriented. Cores were cut into standard specimens (2.5 cm in diameter and 2.2 cm in length).

4.2. Laboratory measurements

Magnetic remanent carrier(s) has already been determined in the two plutons for a detailed AMS study (Charles, 2010). Magnetic mineralogy was investigated by two methods: (1) thermomagnetic measurements carried out at the Institut des Sciences de la Terre d'Orléans (ISTO) and (2) hysteresis loops obtained at the Institut de Physique du Globe de Paris (IPGP). Thermal magnetic (Curie point) experiments were performed with an ©AGICO KLY-3S kappabridge susceptometer coupled with a CS3 furnace. Magnetic hysteresis curves were measured with a magnetic inductometer.

Both thermal and alternating magnetic field (AF) demagnetisations were applied to clean the magnetic remanence at ISTO and IPGP. AF demagnetisation was done using a 2G in-line three-axis AF demagnetiser and the magnetic remanence was measured using a 2G three-axis DC SQUID magnetometer at IPGP. Other samples were demagnetised with a laboratory built furnace and magnetic remanence was measured with an ©AGICO JR-5A automatic spinner magnetometer at ISTO. Inclinations and declinations obtained by

progressive demagnetisations were plotted on orthogonal vector diagrams (Zijderveld, 1967). Magnetic remanence directions were determined by principal component analysis (Kirschvink, 1980). Site-mean directions were computed with Fisher statistics (i.e. Fisher, 1953). Palaeomagnetic software packages of Cogné (2003) and R. Enkin (unpublished) were used for the data analysis.

4.3. Magnetic mineralogy

Representative results of the magnetic mineralogical experiments are presented in Figure 4. Curie temperature measurements for all five measured samples show sharp drop of magnetic susceptibility at around 585°C, characteristic of magnetite (Figs. 4a and 4b; e.g., Dunlop and Özdemir, 1997). A moderate inflexion observed at ~400°C indicates the possible presence of some maghemite (Figs. 4a and 4b). Moreover, in Figure 4b, a drop of magnetic susceptibility occurring between 585°C and 630°C seems to indicate the presence of hematite. Hysteresis loops are particularly narrow-waisted (Figs. 4c and 4d) and present typical low magnetic coercitive multidomain (MD) magnetite grains. The thermomagnetic results, together with magnetic hysteresis curves, indicate that MD magnetite is the dominant magnetic mineral and the main carrier of remanence in all samples for both Weideshan and Haiyang plutons, with possibly a small amount of maghemite and hematite. MD magnetite was directly observed on backscattered electron images with grains reaching 50 µm in length (Figs. 4e and 4f).

4.4. Palaeomagnetic directional analysis

4.4.1. Weideshan pluton

Granodioritic rocks of the Weideshan pluton present unimodal NRM intensities and magnetic susceptibilities ranging from 100 to 1100 $mA.m^{-1}$ and 10 to 70 x 10^{-3} SI with

averages of 343.9 $mA.m^{-1}$ and 33.2 x 10^{-3} SI, respectively. Such high NRM values ensure to perform demagnetisation and to analyse magnetic remanence of these granodioritic rocks.

Typical thermal and AF demagnetisation responses of granodioritic rocks from the Weideshan pluton are presented in Figures 5a and 5b. Overall, the magnetic remanence decays linearly from 150°C to 630°C for thermal demagnetisation and from 4 mT to 100 mT for AF one, with well-defined magnetic component of northward to north-northeastward declinations and downward inclinations. Site-mean directions and the corresponding statistical parameters are listed in Table 1 and Figure 5e. It is noteworthy that three sites (i.e. KW01, KW17 and KW39) show significantly different directions with others rather due to probably the close vicinity to the contact zone which may have experienced a higher cooling rate and border deformation effect (specified by * in Table 1). Moreover, the mean direction of site KW14 may be influenced by the secular variation due to weak number of samples (only three; specified by *** in Table 1). Consequently, these four sites are excluded from site-mean direction calculation for the Weideshan pluton (Table 1). Thus a mean direction was calculated for the Weideshan pluton from nine out thirteen sites: D = 11.3°, I = 61.0°, k = 59.5 and α_{95} = 6.7 (Table 1 and Fig. 5e).

4.4.2. Haiyang pluton

Natural remanent magnetisation (NRM) intensities for granitic rocks of the Haiyang pluton range from 30 to 1200 $mA.m^{-1}$ with average of 375.5 $mA.m^{-1}$. Magnetic susceptibility values range between 25 and 60000 x 10^{-6} SI with average of 23200 x 10^{-6} SI, which is typical of ferromagnetic granitoids (Bouchez, 1997, 2000). The rather high NRM values allow to perform magnetic remanence measurements and, then, to isolate the palaeomagnetic directions acquired during pluton cooling.

Figures 5c and 5d present representative behaviours of measured specimens for thermal and AF demagnetisations. For most of the sites, after the removal of random components up to ~150°C and 2 mT, the magnetic remanent directions become stable. The magnetic remanence decays linearly to the origin until 630°C and 100 mT. The magnetic remanent directions are characterised by downward inclinations with northward declinations. The magnetic directions within each site are well-grouped except for three sites that show dispersed individual directions with high α_{95} and low k values (i.e. KH50, KH57 and KH58; specified by ** in Table 1). A possible origin of scattered directions is discussed in Section 5.1. Consequently, mean directions were computed by Fisher statistics from eleven out fourteen sites. Mean direction calculated for the Haiyang pluton is: D = 1.5°, I = 57.0°, k = 60.2 and α_{95} = 6.3° (Fig. 5f and Table 1).

5. Discussion

Thermal and AF demagnetisations have successfully isolated magnetic characteristic components of high temperature and high AF field, mainly carried by MD magnetite with probably small amount of maghemite and hematite. Cluster pluton-mean directions have been obtained from well consistent sites with k > 30 (i.e. 59.5 and 60.2 for Weideshan and Haiyang plutons, respectively), α_{95} < 10° (i.e. 6.7° and 6.3° for Weideshan and Haiyang plutons, respectively). Haiyang and Weideshan plutons show equivalent mean directions with an insignificant angular difference of 6.8° ± 8.9° leading to calculate a mean direction for both plutons on the basis of twenty sites: D = 6.6°, I = 59.8°, k = 51.1 and α_{95} = 4.6° (Fig. 5g and Table 1). Prior to discuss tectonic significations of these new palaeomagnetic data from granodioritic rocks of Jiaodong Peninsula, reliability and age of magnetisation are discussed below.

5.1. Reliability and age of the magnetic remanence

For the Haiyang pluton, new acquired age data yielded a narrow ~2.5 Ma time difference between U/Pb age on zircon and $^{40}Ar/^{39}Ar$ age on biotite which is well in line with an emplacement in the upper crust. This difference is interpreted as the time elapsed during cooling from about 800 ± 50°C down to about 300 ± 30°C, according to the mineral closure temperatures (Harrison et al., 1985; Villa, 1998; Cherniak and Watson, 2000). Magnetic remanence was acquired by the MD magnetite grains during this fast cooling history of the Haiyang intrusion and the age of magnetisation must, therefore, lie between 117.8 ± 2.7 Ma and 115.4 ± 1.2 Ma. Direct dating of magnetic remanence by hornblende $^{40}Ar/^{39}Ar$ analysis whose closure temperature lies in the same temperature range unluckily failed. Assuming a linear decrease of temperature, age data are plotted on a temperature/time (T-t) diagram (Fig. 6) in order to estimate tentatively the magnetic remanence age of the Haiyang pluton (Fig. 6). Using magnetic unblocking temperatures for MD magnetite between 560 and 585°C, a magnetic remanence age of about 116.0 ± 1.8 Ma for the Haiyang pluton is proposed. As far as the Weideshan pluton is concerned, 118 ± 2 Ma U/Pb age on zircon (Zhang et al., 2007) appears amazingly strictly coeval with the Haiyang pluton (117.8 ± 2.7 Ma). A main magmatic pulse is thus observed in the whole region supported by the geochronological data (e.g., Wang et al., 1998; Wu et al., 2005a), the obvious petrographic and geochemical similarities of the plutons (SBGMR, 1991). While $^{40}Ar/^{39}Ar$ ages is currently lacking for the Weideshan pluton, it is tempting to assume similar fast cooling rates of the same order; the involved magnetic remanence age for the Weideshan pluton would also be settled at 116.0 ± 1.8 Ma (Fig. 6).

Age of magnetisation for both plutons is thus consistent with the Cretaceous Normal Superchron (CNS) period between ~118 and 83 Ma (Gradstein et al., 2004) and the absence of reverse polarities in our palaeomagnetic collection. Moreover, the magnetic unblocking

temperature interval considered for magnetite (560-585°C) and the fast cooling rate, involve a duration of the remanent acquisition of about 120,000 years. Consequently, we assume that secular variation is broadly averaged out for sites of both plutons. However, seven palaeomagnetic sites (i.e. KW01, KW14, KW17, KW39, KH50, KH57 and KH58) reveal dispersed directions and have been excluded for mean calculation (Table 1). In fact, palaeomagnetic sampling that covers a large area within plutons allows to access to different structural levels since the elevation variations reach several hundred meters. Three excluded sites (i.e. KW01, KW14 and KW39; specified by * in Table 1) are located in close vicinity to the pluton envelope with respect to country rocks associated with a presumed fast and more heterogeneous cooling (<10,000 yr), impeding to average the secular variation. Site KW14 (specified by *** in Table 1) has been excluded due to weak number of samples (3 cores) impeding to average the secular variation too. The last three excluded sites (i.e. KH50, KH57 and KH58; specified by ** in Table 1) are poorly statistically defined with high α_{95} and low k values. Besides, structural and AMS studies have shown that both plutons have not experienced any significant deformation subsequently to their emplacement (Charles, 2010), nor any rotation along a horizontal axis.

The characteristic magnetic remanence isolated from granodiorite of both plutons can be confidently considered as primary thermal magnetisations and, therefore, used for tectonic applications. Two palaeomagnetic poles have been thus calculated for the Weideshan pluton (λ = 80.1°N, Φ = 180.1°E, A_{95} = 9.0° with N = 9) and Haiyang pluton (λ = 86.5°N, Φ = 161.1°E, A_{95} = 8.9° with N = 11), respectively (Table 4 and Fig. 7a).

5.2. Is there Cretaceous rotation(s) within Jiaodong Peninsula?

Fifteen palaeomagnetic poles, including results of this study, are available for the Jiaodong Peninsula in Table 4 and Figures 7a with corresponding declinations presented in

Figure 7b. Among them, three poles from Huang et al. (2007) are distinguishable by abnormal northeastward declination with respect to the others (specified in Table 4 by *; see also Fig. 7). These three poles, measured from andesitic rocks of the Qingshan Group, are located in the southern and easternmost parts of Jiaodong Peninsula, close to the Muping-Jimo fault (MJF; see Fig. 2 in Huang et al., 2007). According to their study, age of remanence for these three poles spans between ~125-118 Ma. Thus such northeastward declinations have led the authors to suggest a relative clockwise (CW) rotation of the southern and easternmost parts of Jiaodong Peninsula with respect to the other sites from the same peninsula and NCB as well, since mid-Early Cretaceous (Huang et al., 2007). However, our new palaeomagnetic results from two granodioritic plutons located to the east of MJF present rather consistent directions, for inclination and declination, with those from the west of MJF, but significantly different from these three previous discussed poles (Table 4 and Fig. 7). This difference can be probably explained by two main reasons: (1) the short magnetisation time and (2) the vicinity of the palaeomagnetic sampling sites with respect to main fault zones. In addition, these three poles are derived from volcanics of the Qingshan Group whose cooling ages are constrained by $^{40}Ar/^{39}Ar$ means to 125-118 (Qiu et al., 2001; Song and Wang, 2003; Zhang et al., 2003). Since sampled rocks of these poles (specified in Table 4 by *) are andesites, it is highly questionable if secular variations have been averaged from these palaeomagnetic measurements to ensure an axial-centred-dipolar field as the hypothesis for the application of the palaeomagnetism to the plate tectonics. Furthermore, two of these latter three results are obtained from zones close to the Muping-Jimo Fault (MJF; Fig. 7b) whose motion has been recently constrained at 122.8 ± 0.3 Ma (Zhang et al., 2007; Fig. 1b) by $^{40}Ar/^{39}Ar$ analyses on synkinematic biotites. Deformation (e.g., motion over the fault zone) then appears of coeval with andesite emplacement (~125-118 Ma; Qiu et al., 2001; Song and Wang, 2003; Zhang et al., 2003). Consequently, these zones may have experienced local faulting/deformation-

related rotations along the MJF. Moreover, the remained rotated palaeomagnetic pole (also from andesite) is issued from a small basin located in the easternmost part of the peninsula, to the north of the Weideshan pluton (Huang et al., 2007; Figs. 1b and 7b). Field observations revealed that the scarce outcrops are often highly weathered and are affected by brittle faulting likely to produce local yet important rotations. Furthermore, the initial geometry of the bedding may be also questionable as these sediments are thought to be syntectonic. According to (1) a good consistency between most of the palaeomagnetic results from both sides of the MJF, (2) questions on secular variations and local rotations, these three poles may not be applied to Jiaodong Peninsula-scaled tectonics. Consequently, the good consistency among all poles from the Jiaodong Peninsula (except for three discussed above) illustrate that there is no significant palaeomagnetic evidence for a relative rotation or movement within the Jiaodong Peninsula and therefore, a Cretaceous age-mean palaeomagnetic pole has been calculated at λ ($K_{1\text{-}2}$) = 84.7°N, Φ ($K_{1\text{-}2}$) = 191.3°E, A_{95} = 5.3° with n = 12 (Table 4 and Fig. 7a). This observation confirms also the Cretaceous stationary kinematic nature of China blocks (NCB and SCB; Enkin et al., 1991).

5.3. Relative motions between rigid blocks and tectonic implications for eastern Asia

Eastern Asia appears as a landmass formed by the welding of several blocks (e.g., North China block (NCB) and the South China block (SCB)) and experienced a multiphase tectonic evolution as argued by geological evidences and palaeomagnetic studies (e.g., Mattauer et al., 1985; Zhao and Coe, 1987; Sun et al., 1991; Enkin et al., 1992; Okay et al., 1993; Gilder and Courtillot, 1997; Lin et al., 2003; Zhai et al., 2007). During Late Mesozoic times, this region was marked by extensional tectonics and lithospheric thinning (e.g., Menzies et al., 1993; Davis et al., 1996; Ren et al., 2002; Liu et al., 2005; Lin and Wang, 2006; Zhai et al., 2007; Charles et al., 2011). The knowledge of block movements coupled

with geological evidence is of prime importance to better understand their links with continental extension. Indeed, relative motions between blocks seem to play a major role in the development of extensional crustal structures like basins or Metamorphic Core Complexes (MCCs; e.g., Lin et al., 2003; Liu et al., 2005). For instance, relative Cretaceous CW rotation (22.5 ± 10.2°) of the Eastern Liaoning-Korean block (ELKB) with respect to the NCB may be related to the northeast China and southeast Russia sedimentary basins development (e.g., Songliao, Xialiaohe basins) and alternatively, to the South Liaodong and Yiwulüshan MCCs exhumation, (Lin et al., 2003; Liu et al., 2005). Comparison of palaeomagnetic results from the Jiaodong Peninsula with the surrounding blocks may help to recognise the relative movement and tectonic history of this region (e.g., Gilder et al., 1999; Huang et al., 2007). Poles used to discuss the relative motions between Jiaodong Peninsula (JP), Eastern Liaoning-Korean block (ELKB) and North China block (NCB) are presented in Table 4 and Figure 8a.

Palaeomagnetic studies in the ELKB yield five poles for the Early Cretaceous (K_1) and Upper Cretaceous (K_2) which exhibit consistent palaeomagnetic directions (Figs. 8a and 8b). Thus a Cretaceous (K_{1-2}) pole for ELKB was computed at λ (K_{1-2}) = 60.4°N, Φ (K_{1-2}) = 202.4°E, A_{95} = 8.5° with n = 5 (see Lin et al. (2003) for details). Palaeomagnetic data available for the NCB, particularly for Cretaceous age, are compiled in several syntheses (e.g., Enkin et al., 1992; Gilder and Courtillot, 1997; Yang and Besse, 2001). One of their main conclusions is that NCB experienced a stationary period during the Cretaceous and did not experience a palaeomagnetically observable internal relative displacement since the Early Cretaceous (see Table 4 and Fig. 8b for their small confidence error and coherent declination, respectively). The NCB Cretaceous (K_{1-2}) pole used for the following comparison is at λ (K_{1-2}) = 79.5°N, Φ (K_{1-2}) = 198.7°E, A_{95} = 5.2° with n = 7 (Table 4).

Three Cretaceous palaeomagnetic poles from NCB, the Jiaodong Peninsula and Eastern Liaoning-Korea block are presented on Figure 8a. At the first order, they are all

aligned on the small circle centred on the sampling site (JP), indicating the negligible latitudinal motion among them since the Cretaceous. The detailed comparison between the JP pole and the NCB poles reveals a statistically insignificant angular difference of 5.3° ± 7.4°. This angular difference presents a relative latitudinal motion of -0.1° ± 5.9° and a relative rotation of -6.8° ± 9.5° between these two tectonic units at the geographic reference of 37°N and 121°E (Fig. 8a). It infers that the JP did not experienced any significant movement with respect to NCB since Cretaceous though some structures may be locally reactivated by Cenozoic tectonics due to India-Asia collision, implying that the JP can be considered as a rigid part of NCB at least since Cretaceous. Our results are in accordance with previous study of Gilder et al. (1999). Moreover, located to the east of the Tan-Lu fault, the JP shows the consistent palaeomagnetic results with those from the western part, indicating that no any significant latitudinal displacement has taken place along the Tan-Lu fault since Cretaceous. In other words, our results indicate that the sinistral motion along the Tan-Lu fault involved by some authors (e.g., Xu et al., 1987) should have occurred prior to Early Cretaceous. Besides, the comparison of the ELKB pole with that of the NCB exhibits a significant angular difference of 19.1° ± 10.0°, corresponding a significant relative rotation 25.9° ± 13.5°, but an insignificant relative latitudinal movement of 2.7° ± 8.0° at the geographic reference of 42°N and 125°E. Lin et al. (2003) proposed that this CW rotation of the ELKB with respect to the NCB induced the development of northeast China and southeast Russia basins (Fig. 8b). Liu et al. (2005) put forward the role played by the South Liaodong and the Yiwulüshan MCCs to accommodate the CW rotation of the ELKB (Fig. 8b). Based on available absolute time constraints of footwall mylonitic rocks within South Liaodong and Yiwulüshan MCCs at 130-110 Ma, Liu et al. (2005) proposed that most of the CW rotation took place during Early Cretaceous times. Such an accommodation by MCCs exhumation of crustal blocks rotation has been also recognised in the Aegean region (Brun and Sokoutis, 2007). Lin et al. (2003)

proposed that rotation (Euler) pole for ELKB with respect to NCB lies on the southern border of Bohai Bay and immediately to the northwest of the Jiaodong Peninsula (Fig. 8b). Amount of crustal extension thus increases progressively from the Bohai Bay toward the northeast. In the Jiaodong Peninsula, the Guojialing synkinematic pluton was emplaced coevally with ELKB CW rotation (i.e. ~124 Ma, Charles, 2010; Charles et al., 2011) and is located very close to the rotation pole (Figs. 7b and 8b). It is noteworthy that this synkinematic pluton reveals a weaker amount of crustal stretching compared to MCC exhumation, which can explain the insignificant rotation within the Jiaodong Peninsula during Late Early Cretaceous.

This new palaeomagnetic study reveals that the Cretaceous extension in the whole Eastern Asia area appears heterogeneously expressed in time and in space but the proposition of a geodynamic model for this event is beyond the scope of the paper. For instance, geological structures observed and described in the Liaodong and Jiaodong Peninsulas do not reveal the same strain amount undergone by the crust through time (e.g., MCC, synkinematic plutons or sedimentary basins). The ELKB (including Liaodong Peninsula), which has suffered a significant CW rotation with respect to NCB, exhibits a Late Early Cretaceous MCCs exhumation (South Liaodong and Yiwulüshan, ~120-110 Ma; Darby et al., 2004; Liu et al., 2005; Yang et al., 2007; Lin et al., 2008), synkinematic pluton emplacement (Laohushan, ~122 Ma; Lin et al., 2007) and basin infilling (Lin et al., 2003) coeval with the rotation. The Jiaodong Peninsula is characterised by the exhumation of the Linglong MCC during Early Cretaceous times (~143-134 Ma; Charles, 2010; Charles et al., 2011), then followed by syntectonic emplacement of granitic plutons (e.g, Guojialing pluton, ~124 Ma). No rotation has been documented for Jiaodong Peninsula since the late Early Cretaceous and coeval features can be regarded as simple unstrained and intrusive plutons such as the Weideshan and the Haiyang plutons (~118 Ma; Charles, 2010; Charles et al., 2011). Further

investigations are clearly needed to derive a reliable proposition for the mechanisms responsible of the Late Mesozoic extensional event in the whole eastern Asia.

6. Conclusion

Cretaceous kinematic evolution of the Jiaodong Peninsula closely related to the Mesozoic extension of eastern Asia has been palaeomagnetically studied on two granitic plutons whose internal structure (i.e. AMS data) and structural relationships with the country rocks are well observed. Furthermore, U/Pb and $^{40}Ar/^{39}Ar$ radiochronologic methods were performed to accurately constrain the magnetic remanent age and should be regarded as a major feed-back advantage in using granitic rocks for palaeomagnetic study. The multidomain (MD) magnetite has been characterised as the principal magnetic remanent carrier with probably small amount of maghemite and hematite. Cooling rate estimates from geochronological data yielded a magnetic remanent age of ~116 ± 2 Ma, during a relatively fast cooling between ~800°C and ~300°C. The observations of the solo normal magnetic polarity for this palaeomagnetic collection and of the consistent magnetic remanent age with the Cretaceous Normal Superchron (CNS, Gradstein et al., 2004) argue that the characteristic magnetic remanence may be considered as primary. Detailed field observations on the contact between the pluton and country rocks and available AMS data (Charles, 2010) reveal neither any subsequent deformation, nor the rotation along a horizontal axis of the plutons. Furthermore, twenty palaeomagnetic sites from these two plutons show indistinguishable magnetic directions. Among 12 out 15 Cretaceous palaeomagnetic poles, including two from this study, from the Jiaodong Peninsula and on both sides of Tan-Lu and Muping-Jimo faults are statistically consistent, therefore, the deformation within the peninsula may be negligible. The remaining three excluded poles are probably due to the absence of secular variation average or/and the vicinity of fault zones for the palaeomagnetic sampling sites, so they can

not be applied to the Peninsula-scaled tectonics. Comparison between the Cretaceous palaeomagnetic results of the Jiaodong Peninsula and the NCB data set reveal no significative difference. This result indicates that the Jiaodong Peninsula is rigidly part of NCB since, at least, the Cretaceous as suggested by Gilder et al. (1999). In addition, these new palaeomagnetic results confirm that the relative CW rotation of Eastern Liaoning-Korea Block (ELKB) with respect to NCB does not affect the Jiaodong Peninsula. This palaeomagnetic study revealed that the extensional event is heterogeneously expressed in time and space in the Jiaodong Peninsula. For instance, this extension is characterised by Early Cretaceous exhumation of MCC (i.e. Linglong; ~143-134 Ma; Charles, 2010; Charles et al., 2011) followed by emplacement of synkinematic granitic pluton (i.e. Guojialing; 124 Ma) and finally late Early Cretaceous intrusion of unstrained granodioritic plutons (i.e. Weideshan and Haiyang; ~118 Ma). Conversely, in the Liaodong Peninsula, the extension is marked by the opening of the Songliao basin coeval with the emplacement of granitic plutons (e.g., Jiuliancheng pluton, ~156 Ma; Wu et al., 2007), then is followed by the exhumation of MCCs (South Liaodong and Yiwulüshan MCCs, ~120-110 Ma; Yang et al., 2007; Lin et al., 2008) which accommodated CW rotation of the ELKB.

Acknowledgements

This study benefited from a grant in the frame of the French national “Failles-Fluides-Flux” project supported by the INSU-CNRS. The field work was also financed by Chinese projects KZCX2-YW-Q05-05-03, NSFC (90714007 and 40730315). The first author benefited a scholarship grant from the French Minister of Education and Research. We present our special thanks to M. Le Goff and B. Henry for their help during magnetic measurements at the Institut de Physique du Globe de Paris, Chen Ke, Chu Yang and Wang Jun for their assistance on the field. P. Benoist (ISTO) is acknowledged for mineral

separation. Pr. Stuart Gilder and an anonymous reviewer are both greatly acknowledged for their helpful comments to improve our manuscript.

Appendix A. U/Pb analyses on zircon

Zircon crystals were obtained from crushed rock using a combination of heavy liquid and magnetic separation techniques at the Institut des Sciences de la Terre d'Orléans (ISTO). Individual crystals were hand-picked and mounted in the epoxy resin. Experiments were carried out at the (Q)-ICP-MS laboratory of the Institute of Geology and Geophysics, Chinese Academy of Sciences, Beijing. An Agilent 7500a quadruple (Q)-ICPMS was used for simultaneous determination of zircon U/Pb age and trace elements with an attached GeoLas Plus 193 nm excimer ArF laser-ablation system. All the gas lines were purged for over 1 h prior to each analytical session to reduce Pb on the surface to ^{204}Pb <50 cps in the gas blank. The measurements were carried out using time resolved analysis operating in a fast, peak hopping sequence in DUAL detector mode. Rawcount rates for ^{29}Si, ^{204}Pb, ^{206}Pb, ^{207}Pb, ^{208}Pb, ^{232}Th and ^{238}U were collected for age determination. ^{202}Hg is usually <10 cps in the gas blank, therefore the contribution of ^{204}Hg to ^{204}Pb is negligible and is not considered further. The integration time for four Pb isotopes was ~60 ms, whereas for the other isotopes (including ^{29}Si, ^{232}Th and ^{238}U), it was 30 ms. Data were acquired over 30 s with the laser off and 40 s with the laser on, giving ca. 340 (= 170 reading/replicate x2 sweeps) mass scans for a penetration depth of ca. 20 μm. U, Th and Pb concentrations were calibrated by using ^{29}Si as internal standard and NIST SRM 610 as external standard. ^{207}Pb/^{206}Pb and ^{206}Pb/^{238}U ratios were calculated using GLITTER 4.0 (Jackson et al., 2004), which was then corrected using the zircon 91500 as external standard. The ^{207}Pb/^{235}U ratio was calculated from the values of ^{207}Pb/^{206}Pb and ^{206}Pb/^{238}U. Common Pb was corrected according to the method proposed by Andersen (2002). The ^{206}Pb/^{238}U weighted ages and concordia plot were processed using

ISOPLOT 3.1 (Ludwig, 2004). Errors of individual analyses are based on counting statistics and are given at the 1σ level. The detailed procedure can be found in Xie et al. (2008).

Appendix B. Conventional $^{40}Ar/^{39}Ar$ method

Single crystals of biotite were extracted from sample KH283 and progressively degassed using a laser probe. Minerals separated from these two samples were hand-picked under a binocular microscope directly on the rock sample or from the 1000-500 μm fraction after crushing and sieving. Separates were washed in distilled water, acetone and ethanol before the packaging in individual aluminium foil packets for irradiation. Samples were irradiated in the McMaster nuclear reactor (Canada) together with aliquots of MMHb-1 flux monitors (520.4 ± 1.7 Ma; Samson and Alexander, 1987). The samples were irradiated in several batches. The effects of interfering reactions with Ca and K were evaluated using the following correction factors obtained during a previous irradiation (McDougall and Harrison, 1999): $(^{40}Ar/^{39}Ar)_K$ = 0.0156; $(^{39}Ar/^{37}Ar)_{Ca}$ = 0.000651; $(^{36}Ar/^{37}Ar)_{Ca}$ = 0.000254. Single crystals were degassed by means of a defocused continuous 50WCO_2 laser with a beam diameter at least twice the size of the heated grain. After heating and gas cleaning, argon was introduced in a MAP215-250 mass spectrometer with a Nier ion source and a Johnston MM1 electron multiplier, at the Géosciences Montpellier geochronology laboratory. Each analysis involved 5 min for gas extraction and cleaning and 8 min for data acquisition by peak switching from argon mass 40 to 36. Isotopic compositions were estimated by regression on 15 runs. System blanks were evaluated every three experiments. They were in the range of 2 x $10^{-12}cm^3$ for ^{40}Ar, 1.5 x $10^{-14}cm^3$ for ^{39}Ar, 3 x $10^{-15}cm^3$ for ^{38}Ar, 6 x $10^{-14}cm^3$ for ^{37}Ar and 7 x $10^{-15}cm^3$ for ^{36}Ar.

For all analyses, mass discrimination was calculated on the basis of an $^{40}Ar/^{36}Ar$ ratio of 289.0 ± 2.1 for the MAP 215-50 mass spectrometer. For each individual age reported in Table

3, usual isotope corrections including blanks, mass discrimination, radioactive decay of ^{37}Ar and ^{39}Ar and irradiation-induced mass interference were applied. Errors reported for individual steps take into account the errors introduced by these corrections as well as the analytical errors on signals. The uncertainty on the *J*-factor was propagated in the calculation of the error on the total age of each sample, equivalent to a K/Ar age. All ages are given at the one standard deviation (1σ) confidence level.

References

Andersen, T., 2002. Correction of common lead in U-Pb analyses that do not report ^{204}Pb. Chemical Geology 192, 59-79.

Bouchez, J.L., 1997. Granite is never isotropic: an introduction to AMS studies in granitic rocks. In: Bouchez, J.L., Hutton, D.H.W., Stephens, W.E., (eds), Granite: from segregation of melt to emplacement fabrics, Kluwer Academic Publishers, 95-112.

Bouchez, J.L., 2000. Anisotropie de susceptibilité magnétique et fabriques des granites. Compte-Rendus de l'Académie des Sciences de Paris 330, 1-14.

Brun, J.P., Sokoutis, D., 2007. Kinematics of the Southern Rhodope Core Complex (North Greece). International Journal of Earth Sciences 96, 1079-1099.

Charles, N., 2010. Mechanisms of Mesozoic continental extension in East Asia. PhD thesis, Université d'Orléans, 476 p.

Charles, N., Gumiaux, C., Augier, R., Chen, Y., Lin, W., Zhu, R., 2011. Metamorphic Core Complex vs. Synkinematic pluton in continental extension setting: Insights from key structures (Shandong Province, eastern China). Journal of Asian Earth Sciences 40, 261-278.

Chen, Y., Wu, H., Courtillot, V., Gilder, S., 2002. Large N-S convergence at the northern edge of the Tibetan Plateau? New Early Cretaceous paleomagnetic data from Hexi Corrido, NW China. Earth and Planetary Science Letters 201, 293-307.

Chen, L., 2010. Concordant structural variations from the surface to the base of the upper mantle in the North China Craton and its tectonic implications. Lithos, doi:10.1016/j.lithos.2009.12.007.

Cherniak, D.J., Watson, E.B., 2000. Pb diffusion in zircon. Chemical Geology 172, 5-24.

Cogné, J.P., 2003. A Macintosh™ application for treating paleomagnetic data and making plate reconstructions. Geochemical Geophysical Geosystems 4. doi:10.1029/2001GC000227.

Daoudene, Y., Gapais, D., Ledru, P., Cocherie, A., Hocquet, S., Donskaya, T.V., 2009. The Ereendavaa Range (north-eastern Mongolia): an additional argument for Mesozoic extension throughout eastern Asia. International of Earth Sciences (Geol Rundsch), doi: 10.1007/s00531-008-0412-2.

Darby, B.J., Davis, G.A., Zhang, X., Wu, F., Wilde, S., Yang, J., 2004. The newly discovered Waziyu metamorphic core complex, Yiwulüshan, western Liaoning Province, NW China. Earth Science Frontiers 11, 145-155.

Davis, G.A., Qian, X., Zheng, Y., Yu, H., Wang, C., Mao, T.H., Gehrels, G.E., Muhammad S., Fryxell, J.E., 1996. Mesozoic deformation and plutonism in the Yunmeng Shan: A Chinese metamorphic core complex north of Beijing, China. In: Yin, A., Harrison, T.A. (eds), The tectonic evolution of Asia. Cambridge University Press, New York, 253-280.

Doh, S., Piper, J., 1994. Paleomagnetism of the Upper Paleozoic-Lower Mesozoic Pyongan Supergroup, Korea: A Phanerozoic link with the North China Block. Geophysical Journal International 117, 850-863.

Donskaya, T.V., Windley, B.F., Mazukabzov, A.M., Kröner, A., Sklyarov, E.V., Gladkochub, D.P., Ponomarchuk, V.A., Badarch, G., Reichow, M.K., Hegner, E., 2008. Age and evolution of late Mesozoic metamorphic core complexes in southern Siberia and northern Mongolia. Journal of Geological Society of London 165, 405-421.

Dunlop, D.J., Özdemir, Ö., 1997. Rock Magnetism, Fundamentals and Frontiers. Cambridge University Press, Cambridge, 573 p.

Eide, E.A., McWilliams, M.O., Liou, J.G., 1994. $^{40}Ar/^{39}Ar$ geochronology and exhumation of high-pressure to ultrahigh-pressure metamorphic rocks in east-central China. Geology 22, 601-604.

Enkin, R.J., Chen, Y., Courtillot, V., Besse, J., Xing, L., Zhang, Z., Zhuang, Z., Zhang, J., 1991. A Cretaceous pole from South China and the Mesozoic hairpin turn of the Eurasian apparent polar wander path. Journal of Geophysical Research 96, 4007-4027.

Enkin, R. J., Yang, Z., Chen, Y., Courtillot, V., 1992. Paleomagnetic constraints on the geodynamic history of the major blocks of China from the Permian to the Present. Journal of Geophysical. Research 97, 13953-13989.

Faure, M., Lin, W., Shu, L., Sun, Y., Schärer, U., 1999. Tectonics of the Dabieshan (E. China) and possible exhumation mechanism of ultra high-pressure rocks. Terra Nova 11, 251-258.

Faure, M., Lin, W., Le Breton, N., 2001. Where is the North China-South China block boundary in eastern China? Geology 29, 119-122.

Faure, M., Lin, W., Monié, P., Le Breton, N., Poussineau, S., Panis, D., Deloule, E., 2003. Exhumation tectonics of the ultrahigh-pressure metamorphic rocks in the Qinling orogen in east China: New petrological-structural-radiometric insights from the Shandong Peninsula: Tectonics 22, 1018, doi:10.1029/2002TC001450.

Fisher, R., 1953. Dispersion on a sphere. Proceedings of the Royal Society of London: Series A 217, 295-305.

Gilder, S.A., Keller, G.R., Luo, M., Goodell, P.C., 1991. Timing and spatial distribution of rifting in China. Tectonophysics 197, 225-243.

Gilder, S., Courtillot, V., 1997. Timing of the north-south China collision from new middle to late Mesozoic paleomagnetic data from the North China Block. Journal of Geophysical Research 102, 17713-17727.

Gilder, S., Leloup, P., Courtillot, V., Chen, Y., Coe, R., Zhao, X., Xiao, W., Halim, N., Cogné, J.P., Zhu, R., 1999. Tectonic evolution of of the Tancheng-Lujiang (Tan-Lu) fault via Middle Triassic to Early Cenozoic palaeomagnetic data. Journal of Geophysical Research 104, 15365-15390.

Gradstein, F.M., Ogg, J.G., Smith, A.G., et al., 2004. A geologic time scale 2004. International Commission on Stratigraphy (ICS), Cambridge University Press.

Griffin, W.L., Andi, Z., O'Reilly, S.Y., Ryan, C.G., 1998. Phanerozoic evolution of the lithosphere beneath the Sino-Korean craton. In: Flower, M., Ching, S.L., Lo, C.H., Lee, T.Y. (Eds), Mantle dynamics and plate interactions in East Asia. AGU Geodynamics Series 27, 107-126.

Hacker, B.R, Ratschbacher, L., Webb, L., Ireland, T., Walker, D., Dong, S., 1998. U/Pb zircon ages constrain the architecture of the ultrahigh-pressure Qinling-Dabie orogen, China. Earth Planetary Science Letters 161, 215-230.

Harrison, T.M., Duncan, I., McDougall, H., 1985. Diffusion of ^{40}Ar in biotite: temperature, pressure and compositional effects. Geochimica Cosmochimica Acta 49, 2461-2468.

Huang, B., Piper, J.D.A., Zhang, C., Li, Z., Zhu, R., 2007. Palaeomagnetism of Cretaceous rocks in the Jiaodong Peninsula, eastern China: Insights into blocks rotations and neotectonic deformation in eastern Asia. Journal of Geophysical Research 112, B03106, doi:10.1029/2006JB004462.

Jackson, S.E., Pearson, N.J., Griffin, W.L., Belousova, E.A., 2004. The application of laser ablation inductively coupled plasma-mass spectrometry (LA-ICP-MS) to in situ U-Pb zircon geochronology. Chemical Geology 211, 47-69.

Jelinek, V., 1981. Characterization of the magnetic fabric of rocks. Tectonophysics 79, 63.

Kirschvink, J.L., 1980. The least squares line and the analysis of palaeomagnetic data. Geophysical Journal of the Royal Astonomical Society 62, 699-718.

Kusky, T., Windley, B.F., Zhai, M.G., 2007. Tectonic evolution of the North China Block: from orogen to craton to orogen. In: Zhai, M.G., Windley, B.F., Kusky, T., Meng, Q.R. (Eds), Mesozoic sub-continental lithospheric thinning under eastern Asia. Geological Society of London, Special Publications 280, 1-34.

Lee, G., Besse, J., Courtillot, V., Montigny, R., 1987. Eastern Asia on Cretaceous: New paleomagnetic data from South Korea and a new look at Chinese and Japanese data. Journal of Geophysical Research 92, 3580-3596.

Li, Z., Yang, M., 1993. Geochemistry of Jiaodong gold deposits. Science and Technology Publishing House, Tianjing, 293 p. (in Chinese).

Li, X.H., 2000. Cretaceous magmatism and lithospheric extension in southeast China. Journal of Asian Earth Sciences 18, 293-305.

Lin, W., Faure, M., Monié, P., Schärer, U., Zhang, L., Sun, Y., 2000. Tectonics of SE China, new insights from the Lushan massif (Jangxi Province). Tectonics 19, 852-871.

Lin, W., Chen, Y., Faure, M., Wang, Q., 2003. Tectonic implications of new Late Cretaceous paleomagnetic constraints from Eastern Liaoning Peninsula, NE China. Journal of Geophysical Research 108, doi:10.1029/2002JB002169.

Lin, W., Wang, Q., 2006. Late Mesozoic extensional tectonics in the North China Block: a crustal response to subcontinental mantle removal? Bulletin de la Société Géologique de France 177, 287-294.

Lin, W., Faure, M., Monié, P., Wang, Q.C., 2007. Polyphase Mesozoic tectonics in the eastern part of the North China Blocks: insights from the Liaoning Peninsula massif (NE China). In: Zhai, M.-G., Windley, B.F., Kusky, T.M. & Meng, Q.R. (eds), 2007. Mesozoic sub-continental lithospheric thinning under eastern Asia. Geological Society, London, Special Publications 280, 153-170.

Lin, W., Faure, M., Monié, P., Schärer, U., Panis, D., 2008. Mesozoic extensional tectonics in Eastern Asia : The South Liaodong Peninsula Metamorphic Core Complex (NE China). Journal of Geology 116, 134-154.

Liu, H.F., 1986. Geodynamic scenario and structural styles of Mesozoic and Cenozoic basins in China. American Association of Petrology and Geology Bulletin 70, 377-395.

Liu, B., Wang, X., Cheng, J., Ying, H., 1994. Typical gold deposits in Jiaodong. In: Chen, B. (ed.), New development of research on gold deposits of China 1-1, Chap. 4, Seismological Publishing House, Beijing, 234-258 (in Chinese).

Liu, J., Davis, G., Lin, Z., Wu, F., 2005. The Liaonan metamorphic core complex, southeastern Liaoning Province, North China: A likely contributor to Cretaceous rotation of eastern Liaoning, Korea and contiguous areas. Tectonophysics 407, 65-80.

Ludwig, K.R., 2004. User's manual for ISOPLOT/EX, version 3.1. A geochronological toolkit for ©Microsoft Excel. Berkeley Geochronology Center, Special Publication 4.

Luo, Q., Liu, G., Wang, B., 1992. The research of metamorphic core complex of Hongzhen-Anqing area, Lower Yangtze. Journal of Nanjing University 4, 14-25 (in Chinese with English abstract).

Ma, X., Wu, D., 1987. Cenozoic extensional tectonics in China. Tectonophysics 133, 243-255.

Ma, X., Yang, Z., Xing, L., 1993. The Lower Cretaceous reference pole from the North China and its tectonics implications. Geophysical Journal International 115, 323-331.

Ma, Z., 1997. The comprehensive interpretation report of the gravity and magmatic data in Shandong Province. Institute of prospection and geophysics of the Shandong Province.

Mattauer, M., Matte, P., Malavieille, J., Tapponnier, P., Maluski, H., Xu, Z., Lu, Y., Tang, Y., 1985. Tectonics of Qinling belt: Build-up and evolution of eastern Asia. Nature 317, 496- 500.

Mazukabzov, A.M., Donskaya, T.V., Gladkochub, D.P., Sklyarov, E.V., Ponomarchuk, V.A., Sal'nikova, E.B., 2006. Structure and age of the metamorphic core complex of the Burgutui ridge (Southwestern Transbaikal region). Dokl Earth Sciences 407, 179-183.

McDougall, I., Harrison, T.M., 1999. Geochronology and thermochronology by $^{40}Ar/^{39}Ar$ method, 2nd Ed. Oxford University Press, New York.

Meng, Q., 2003. What drove late Mesozoic extension of the northern China-Mongolia tract? Tectonophysics 369, 155-174.

Menzies, M.A., Fan, W.M., Zhang, M., 1993. Palaeozoic and Cenozoic lithoprobes and the loss of >120 km of Archean lithosphere, Sino-Korean Craton, China, in: Prichard, H.M., Alabaster, T., Harris, N.B.W., Neary, C.R. (eds), Magmatic processes and plate tectonics, Geological Society, London, Special Publications 76, 71-81.

Okada, H., 1999. Plume-related sedimentary basins in East Asia during the Cretaceous. Palaeogeography Palaeoclimatology Palaeoecology 150, 1-11.

Okay, A., Sengör, A., Satir, M., 1993. Tectonics of an ultrahigh-pressure metamorphic terrane: The Dabieshan-Tongbaishan orogen, China. Tectonics 12, 1320-1334.

Pruner, P., 1992. Paleomagnetism and paleogeography of Mongolia from the Carboniferous to Cretaceous. Physics of the Earth and Planetary Interiors 70, 169-177.

Pupin, JP., 1980. Zircon and granite petrology. Contributions to Mineralogy and Petrology 73, 207-220.

Qiu, J., Wang, D., Lo, Q., Liu, H., 2001. $^{40}Ar/^{39}Ar$ dating for volcanic rocks of Qingshan formation in Jiaolai basin, eastern Shandong province: a case study of the Fenlingshan volcanic apparatus in Wulian County. Geological Journal of Chinese University 7, 351-355 (in Chinese with English abstract).

Ren, J., Tamaki, K., Li, S., Junxia, Z., 2002. Late Mesozoic and Cenozoic rifting and its dynamic setting in Eastern China and adjacent areas. Tectonophysics 344, 175-205.

Samson, S.D., Alexander, E.C., 1987. Calibration of the interlaboratory $^{40}Ar/^{39}Ar$ dating standard, MMhb-1. Chemical Geology 66, 27-34.

Sang, L.K., 1984. The origin and evolution of the Linglong granites. Earth Sciences 9, 101-114 (in Chinese).

SBGMR, Shandong Bureau of Geological and Mining Research, 1991. Regional geology of the Shandong Province: Geological Memoirs of Ministry of Geology and Mineral Resources 26, Geological Publishing House, Beijing, 699 p., (in Chinese).

Song, C.M., Yan, Q.L., 2000. Characteristics of dioritic inclusions in Weideshan superunit and its magma origin in Jiaonan area. Shandong Geology 4, 16-21.

Song, C.M., Wang, P.C. (eds), 2003. Regional geology of Shandong Province, 970 p., Map Publushing House of Shandong, Jinan, China.

Spear, F.S., 1993. Metamorphic phase equilibria and pressure-temperature time paths. Mineralogy Society of America, Washington D.C., 799 p.

Sun, S., Li, J., Lin, J., Wang, Q., Chen, H., 1991. Indosinides in China and the consumption of eastern paleotethys. In: Muller, D.W., McKenzie, J.A., Weissert, H. (eds), Controversies in Modern Geology, p. 363-384, Academic, San Diego, California.

Tera, F., Wasserburg, G.J., 1972. U-Th-Pb systematics in three Apollo 14 basalts and the problem of initial Pb in lunar rocks. Earth Planetary Sciences Letters 14,281-304.

Uchimara, H., Kono, M., Tsunawaka, H., Kimura, G., Wei, Q., Hao, T., Liu, H., 1996. Palaeomagnetism of late Mesozoic rocks from northeastern China: The role of the Tan-Lu fault in the North China Block. Tectonophysics 262, 301-319.

Villa, I.M., 1998. Isotopic closures. Terra Nova 10, 42-47.

Wang, L.G., Qiu, Y.M., McNaughton, N.J., Groves, D.I., Luo, Z.K., Huang, J.Z., Miao, L.C., Liu, Y.K., 1998. Constraints on crustal evolution and gold metallogeny in the Northwestern Jiaodong Peninsula, China, from SHRIMP U-Pb zircon studies of granitoids. Ore Geology Reviews 13, 275-291.

Wang, F., Zhou X.-H., Zhang, L.-C., Ying, J.-F., Zhang, Y.-T., Wu, F.-Y., Zhu, R.-X., 2006. Late Mesozoic volcanism in the Great Xing'an Range (NE China): Timing and implications for the dynamic setting of NE Asia. Earth and Planetary Science Letters 251, 179-198.

Watson, M.P., Hayward, A.B., Parkinson, D.N., Zhang, Z.M., 1987. Plate tectonic history, basin development and petroleum source rock deposition onshore China. Marine Petroleum Geology 4, 205-225.

Webb, L.E., Graham, S.A., Johnson, C.L., Badarch, G., Hendrix, S., 1999. Occurrence, age, and implications of the Yagan-Onch Hayrhan metamorphic core complex, southern Mongolia. Geology 27, 143-146.

Wu, F.Y., Lin, J.Q., 1991. Weideshan plutonic complex, an example of magmatic pulsating crystallization. Journal of Changchun University of Earth Science 21, 291-299 (in Chinese with English abstract).

Wu, H., Zhou, L., Zhao, Z., Yang, Z., Chen, Y., 1993. Paleomagnetic results of the late Paleozoic and Mesozoic from the Alashan area of the north-western China Block. Scientia Geologica Sinica 2, 19-46.

Wu, F.Y., Lin, J., Wilde, S.A., Zhang, X., Yang, J., 2005a. Nature and significance of the Early Cretaceous giant igneous event in eastern China. Earth and Planetary Science Letters 233, 103-119.

Wu, F.Y., Yang, J.H., Wilde, S.A., Zhang, X.O., 2005b. Geochronology, petrogenesis and tectonic implications of the Jurassic granites in the Liaodong Peninsula, NE China. Chemical Geology 221, 127-156.

Wu, F.Y., Han, R.H., Yang, J.H., Wilde, S.A., Zhai, M.G., Park, S.C., 2007. Initial constraints on the timing of granitic magmatism in North Korea using U-Pb zircon geochronology. Chemical Geology 238, 232-248.

Xie, L.W., Zhang, Y.B., Zhang, Y.H., Sun, J.F., Wu, F.Y., 2008. In situ simultaneous determination of trace elements, U-Pb and Lu-Hf isotopes in zircon and baddeleyite. Chinese Science Bulletin 53, 1565-1573.

Xu, J., Zhu, G., Tong, W., Cui, K., Liu, Q., 1987. Formation and evolution of the Tancheng-Lujiang wrench fault system: A major shear system to the northwest of the Pacific Ocean. Tectonophysics 134, 273-310.

Yan, J., Chen, J.F., Xie, Z., Zhou, T.X., 2003. Mantle xenoliths from Late Cretaceous basalt in eastern Shandong Province: New constraint on the timing of lithospheric thinning in eastern China. Chinese Science Bulletin 48, 2139-2144.

Yang, M., Lü, G., 1996. The geology-geochemistry of gold deposits of the greenstone belt in Jiaodong district. Geological Publishing House, Beijing, pp.228 (in Chinese with English abstract).

Yang, Z., Besse, J., 2001. New Mesozoic apparent polar wander path for south China: Tectonic consequence. Journal of Geophysical Research 106, 8493-8520.

Yang, J.H., Wu, F.Y., Chung, S.L., Lo, C.H., Wilde, S.A., Davis, G.A., 2007. Rapid exhumation and cooling of the Liaonan metamorphic core complex: Inferences from $^{40}Ar/^{39}Ar$ thermochronology and implications for Late Mesozoic extension in the eastern North China Craton. Geological Society of America Bulletin 119, 1405-1414.

Yu, J.X., 1990. Study of Early Cretaceous angiosperm spores in north China. Thesis collection of stratigraphic palaeontology 23, 212-228, Geological Publishing House, Beijing (in Chinese).

Zhai, M.G., Windley, B.F., Kusky, T.M., Meng, Q.R. (eds), 2007. Mesozoic sub-continental lithospheric thinning under eastern Asia. Geological Society, London, Special Publications 280.

Zhang, Y.Q., Dong, S.W., Shi, W., 2003. Cretaceous deformation history of the middle Tan-Lu fault zone in Shandong Province, eastern China. Tectonophysics 363, 243-258.

Zhang, H.Y., Hou, Q.L., Cao, D.Y., 2007. Tectono-chronologic constraints on a Mesozoic slip and thrust belt in the eastern Jiaodong Peninsula. Science in China Series D 50, 25-32.

Zhao, X., Coe, R., 1987. Paleomagnetic constraints on the collision and rotation of north and south China. Nature 327, 141- 144.

Zhao, X., Coe, R., Zhou, Y., Wu, H., Wang, J., 1990. New palaeomagnetic results from northern China: Collision and suturing with Siberia and Kazakhstan. Tectonophysics 181, 43-81.

Zhao, X., Coe, R., Chang, K., Park, S., Omarzai, S. Zhu, R., Zhu, Y., Gilder, S., Zheng, Z., 1999. Clockwise rotations recorded in Early Cretaceous rocks of South Korea: Implications for tectonic affinity between the Korean Peninsula and North China. Geophysical Journal International 138, 447-463.

Zheng, S., Kono, M., Tsunakawa, H., Kimura, G., Wei, Q., Zhu, X., Hao, T., 1991. The apparent polar wander path for the North China Block since the Jurassic. Geophysical Journal International 104, 29-40.

Zhou, X.M., Li, W.X., 2000. Origin of Late Mesozoic igneous rocks in southeastern China: implications for lithospheric subduction and underplating of mafic magmas. Tectonophysics 326, 269-287.

Zhou, T., Lü, G., 2000. Tectonics, granitoids and Mesozoic gold deposits in East Shandong, China. Ore Geology Reviews 16, 71-90.

Zijderveld, J.D.A., 1967. AC demagnetisation of rocks: analysis of results. In: Collinson, D.W., Creer, K.M., Runcorn, S.K. (eds), Methods on Paleomagnetism. Elsevier, 245-286.

Figure captions

Figure 1: (a) Tectonic sketch of eastern Asia. Sulu UHP B.: Sulu Ultra-High Pressure Belt; TNCB: Trans-North China Belt; TLF: Tan-Lu Fault. (b) Simplified geological map of Jiaodong Peninsula (Shandong Province). LJ: Luanjiahe pluton; GJL: Guojialing synkinematic pluton; SF: Sanfoshan pluton; HY: Haiyang pluton; WD: Weideshan pluton; KY: Kunyushan pluton; WG: Wendeng pluton; AI: Aishan pluton. U/Pb on zircon ages come from Wang et al. (1998); Zhang et al. (2007). $^{40}Ar/^{39}Ar$ ages after Charles (2010). LDF: Linglong detachment fault; GSZ: Guojialing shear zone. (1) is the Muping-Jimo fault, (2) Rushan-Weihai fault, (3) Haiyang-Rongcheng fault and (4) Haiyangsu-Shidao fault (Huang et al., 2007).

Figure 2: (a) and (b) Structural maps of Weideshan and Haiyang plutons with the location of the palaeomagnetic sampling sites and samples used for the geochronological study. AMS foliation trajectories are issued from Charles (2010). (c) and (d) Equal-area projection of AMS data for both plutons with K_1 (AMS lineation in grey squares) and K_3 (AMS pole to foliation in white circles) mean direction. (e) T (shape parameter) vs. P_J (corrected anisotropy degree) for both plutons (Charles, 2010).

Figure 3: (a) CL images of representative zircons. Shown are locations of analytical points. The diameter of ablation pit is ca. 30 μm. (b) Tera and Wasserburg Concordia diagram for Haiyang granodiorite (07-056; Tera and Wasserburg, 1972). Data-point error ellipses are

plotted as 1σ. (c) Al^{IV} vs. Fe/(Fe+Mg) classification for analysed biotites for $^{40}Ar/^{39}Ar$ analyses (see Table 2 for details). (d) Biotite $^{40}Ar/^{39}Ar$ age spectrum of the Haiyang granodiorite (KH283). Errors are given with 1σ. See Table 3 for details. TFA = Total Fusion Age. bi : biotite.

Figure 4: Results of the magnetic mineralogical investigation for Weideshan and Haiyang granodioritic plutons. (a) and (b) Thermomagnetic measurements; black and grey curves indicate heating and cooling stages, respectively. (c) and (d) Hysteresis cycles showing typical shape for ferromagnetic minerals. Paramagnetic corrections have been applied to the loops. Modified from Charles (2010).

Figure 5: Magnetic remanent measurements and palaeomagnetic results from the Weideshan and Haiyang plutons. (a) to (d) Orthogonal projection of sample demagnetisation (T and F for thermal and AF demagnetisations, respectively; Zijderveld, 1967). Black and white circles represent horizontal and vertical plans, respectively. (e) to (f) Equal-area projection for site-mean directions isolated from high temperature and high coercitive AF components in geographic coordinates. Stars represent the pluton-mean directions.

Figure 6: Temperature/time diagram showing the inferred cooling path for both plutons and estimated age of magnetic remanence of magnetite. U/Pb age for Weideshan comes from Zhang et al. (2007).

Figure 7: (a) Equal-area projection of available Cretaceous palaeomagnetic poles for the Jiaodong Peninsula and (b) the corresponding palaeodeclination map. Star presents the Cretaceous average without three poles in grey colour (see the text for the details). Fault

abbreviations: TLF: Tan-Lu fault, MJF: Muping-Jimo fault, RWF: Rushan-Weihai fault and HRF: Haiyang-Rongcheng fault.

Figure 8: (a) Equal-area projection of mean Cretaceous poles for Jiaodong Peninsula (JP), North China Block (NCB) and Eastern Liaoning-Korean Block (ELKB), with angular differences of JP and ELKB with respect to NCB. Grey star represents sampling location of this study. Small circle centered on this location and passing through poles reveals a negligible relative palaeolatitudinal movement among these blocks since the Cretaceous. (b) Palaeodeclination map of North China with principal tectonic structures. Block abbreviations: NCB: North China block, SCB: South China block, ELKB: Eastern Liaoning-Korean block, JP: Jiaodong Peninsula. Fault abbreviation: TLF: Tan-Lu fault. Extensive domes abbreviations: BU: Buteel-Burgutoy (Mazukabzov et al., 2006; Donskaya et al., 2008), ED: Ereendavaa (Daoudene et al., 2009), GD: Gudaoling (Charles, 2010), HG: Hongzhen (Luo et al., 1992), LL: Linglong (Charles et al., **2011**), LS: Lushan (Lin et al., 2000), LU: Luotian (Eide et al., 1994; Hacker et al., 1998; Faure et al., 1999), SL: South Liaodong (Liu et al., 2005), YA: Yagan-Onch Hayrhan (Zheng et al., 1991; Webb et al., 1999), YU: Yunmengshan (Davis et al., 1996), YW: Yiwulüshan (Darby et al., 2004), ZA: Zagan (Donskaya et al., 2008).

Tables

Table 1: GPS position of the sampling sites and palaeomagnetic directions for Weideshan and Haiyang plutons. Abbreviations: n, number of samples taken into statistic calculation; N, number of measured samples; D, I, declination and inclination, respectively; k: the precision parameter; α_{95}: the radius that the mean direction lies within 95% confidence. The sites in

italic are excluded from mean calculations (*: site located close to the pluton border, **: site poorly statistically defined with high α_{95} and low k values, ***: site with weak sampling).

Table 2: Details of U/Pb analyses on zircons of the Haiyang granodioritic pluton after data reduction and common Pb corrections. Uncertainties are at 1σ, including the error related to calibration.

Table 3: Details of $^{40}Ar/^{39}Ar$ of analyses performed on biotites of the Haiyang granodioritic pluton.

Table 4: Compilation of Cretaceous palaeomagnetic data of North and eastern China. Abbreviations: N, the number of sites; Slat (Plat), the latitude of sampling site (pole); Slong (Plong), the longitude of sampling site (pole); A_{95}, the radius that mean pole lies within 95% confidence, in degree. The palaeomagnetic poles denoted by * are eliminated from the average.

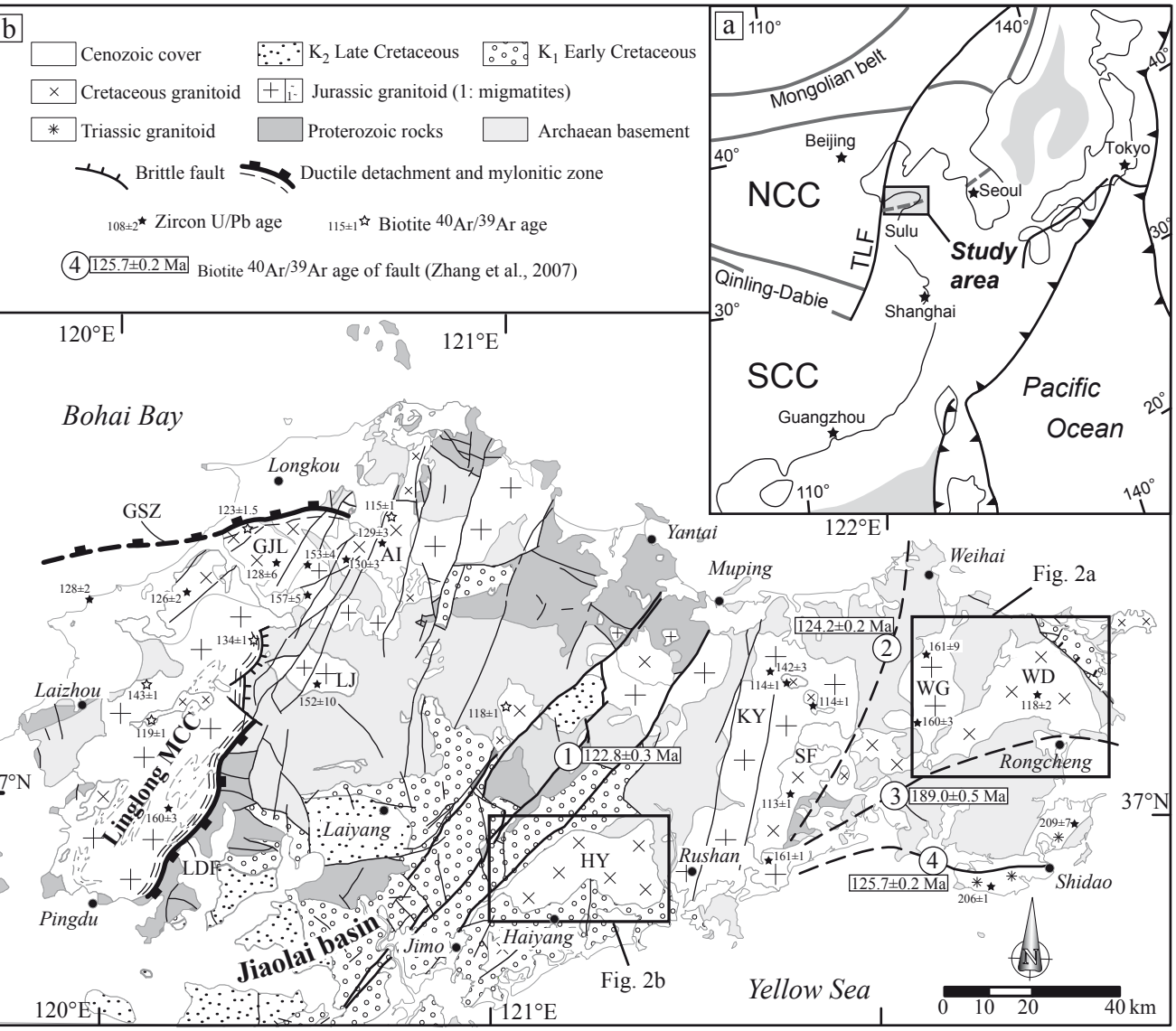
b
Cenozoic cover
K2 Late Cretaceous
K1 Early Cretaceous
Cretaceous granitoid
Jurassic granitoid (1: migmatites)
Triassic granitoid
Proterozoic rocks
Archaean basement
Brittle fault
Ductile detachment and mylonitic zone
108±2 Zircon U/Pb age
115±1 Biotite 40Ar/39Ar age
4 125.7±0.2 Ma Biotite 40Ar/39Ar age of fault (Zhang et al., 2007)
a
110°
140°
40°
30°
20°
Mongolian belt
Beijing
Tokyo
Seoul
NCC
Sulu
TLF
Study area
Qinling-Dabie
Shanghai
SCC
Pacific Ocean
Guangzhou
120°E
121°E
122°E
Bohai Bay
Longkou
GSZ
123±1.5
115±1
129±3
GJL
153±4
AI
130±3
128±6
126±2
157±5
128±2
134±1
Yantai
Muping
Weihai
Fig. 2a
124.2±0.2 Ma
2
161±9
WG
WD
118±2
160±3
142±3
114±1
114±1
LJ
143±1
152±10
Laizhou
119±1
118±1
KY
SF
1 122.8±0.3 Ma
Linglong MCC
Rongcheng
3 189.0±0.5 Ma
37°N
113±1
209±7
Laiyang
HY
Rushan
161±1
4
125.7±0.2 Ma
Shidao
206±1
LDF
Pingdu
Jiaolai basin
Jimo
Haiyang
Fig. 2b
Yellow Sea
N
0 10 20 40 km

Figure 1

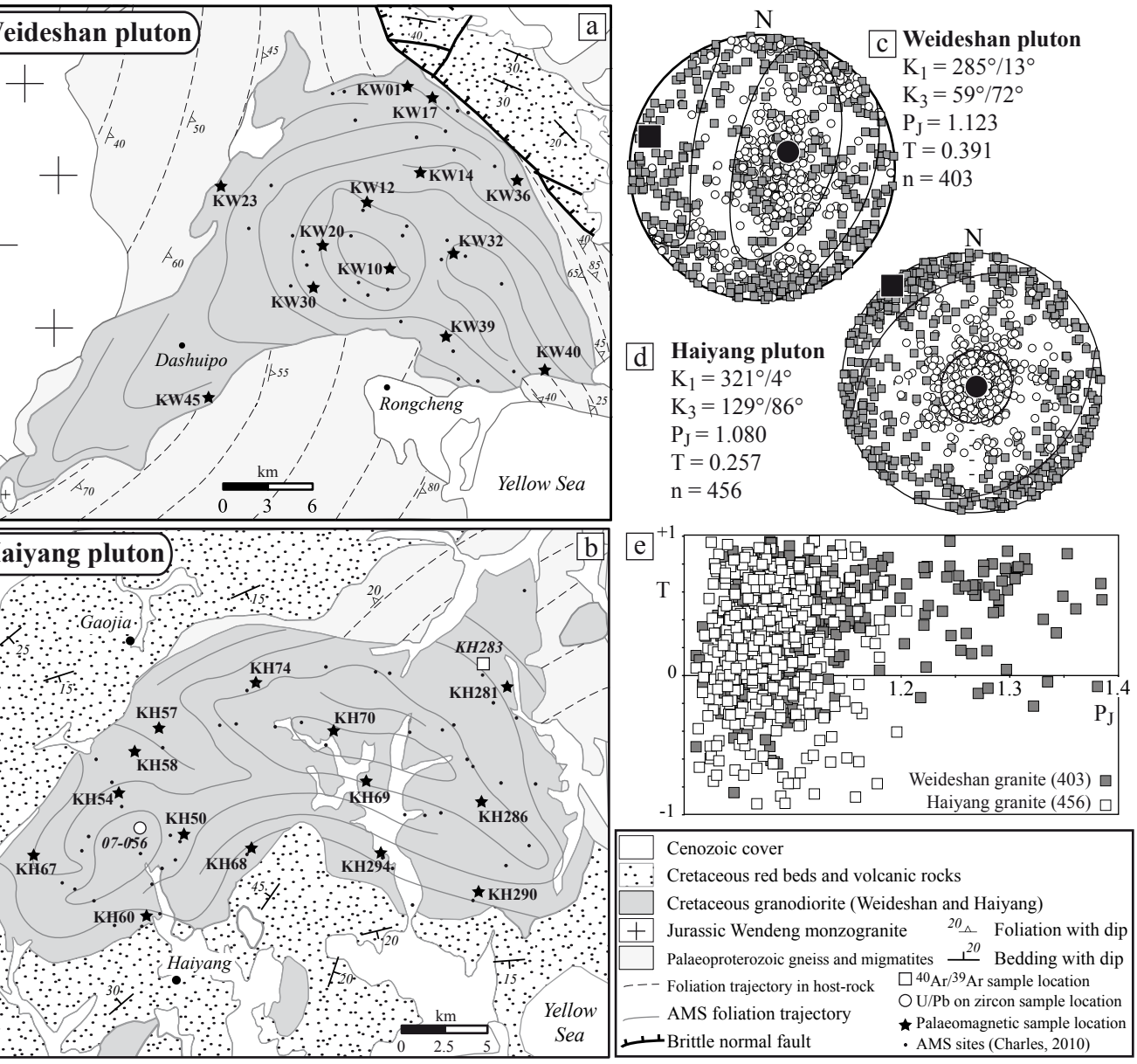
a
Weideshan pluton
KW01
KW17
KW14
KW12
KW23
KW36
KW20
KW32
KW10
KW30
KW39
KW40
KW45
Dashuipo
Rongcheng
Yellow Sea
km
0 3 6
b
Haiyang pluton
Gaojia
KH283
KH74
KH281
KH57
KH70
KH58
KH54
KH69
KH286
KH50
07-056
KH67
KH68
KH294
KH290
KH60
Haiyang
Yellow Sea
km
0 2.5 5
c
Weideshan pluton
K1 = 285°/13°
K3 = 59°/72°
PJ = 1.123
T = 0.391
n = 403
N
d
Haiyang pluton
K1 = 321°/4°
K3 = 129°/86°
PJ = 1.080
T = 0.257
n = 456
N
e
+1
T
0
-1
1.2
1.3
1.4
PJ
Weideshan granite (403)
Haiyang granite (456)
Cenozoic cover
Cretaceous red beds and volcanic rocks
Cretaceous granodiorite (Weideshan and Haiyang)
Jurassic Wendeng monzogranite
Palaeoproterozoic gneiss and migmatites
Foliation trajectory in host-rock
AMS foliation trajectory
Brittle normal fault
Foliation with dip
Bedding with dip
40Ar/39Ar sample location
U/Pb on zircon sample location
Palaeomagnetic sample location
AMS sites (Charles, 2010)

Figure 2

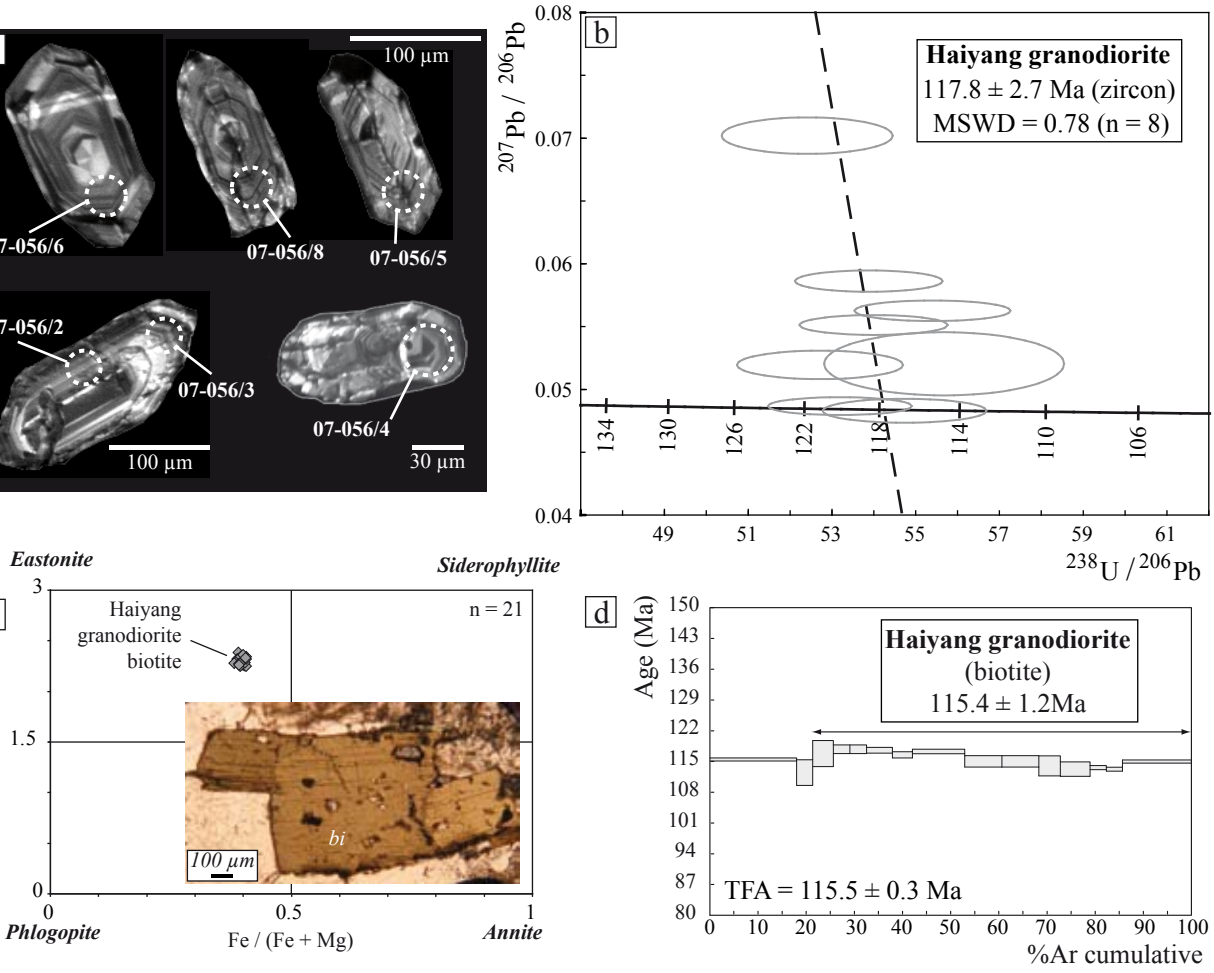
100 µm
07-056/6
07-056/8
07-056/5
07-056/2
07-056/3
07-056/4
100 µm
30 µm
b
Haiyang granodiorite
117.8 ± 2.7 Ma (zircon)
MSWD = 0.78 (n = 8)
207Pb / 206Pb
238U / 206Pb
Eastonite
Siderophyllite
Haiyang granodiorite biotite
n = 21
100 µm
bi
Phlogopite
Annite
Fe / (Fe + Mg)
d
Haiyang granodiorite
(biotite)
115.4 ± 1.2Ma
TFA = 115.5 ± 0.3 Ma
Age (Ma)
%Ar cumulative

Figure 3

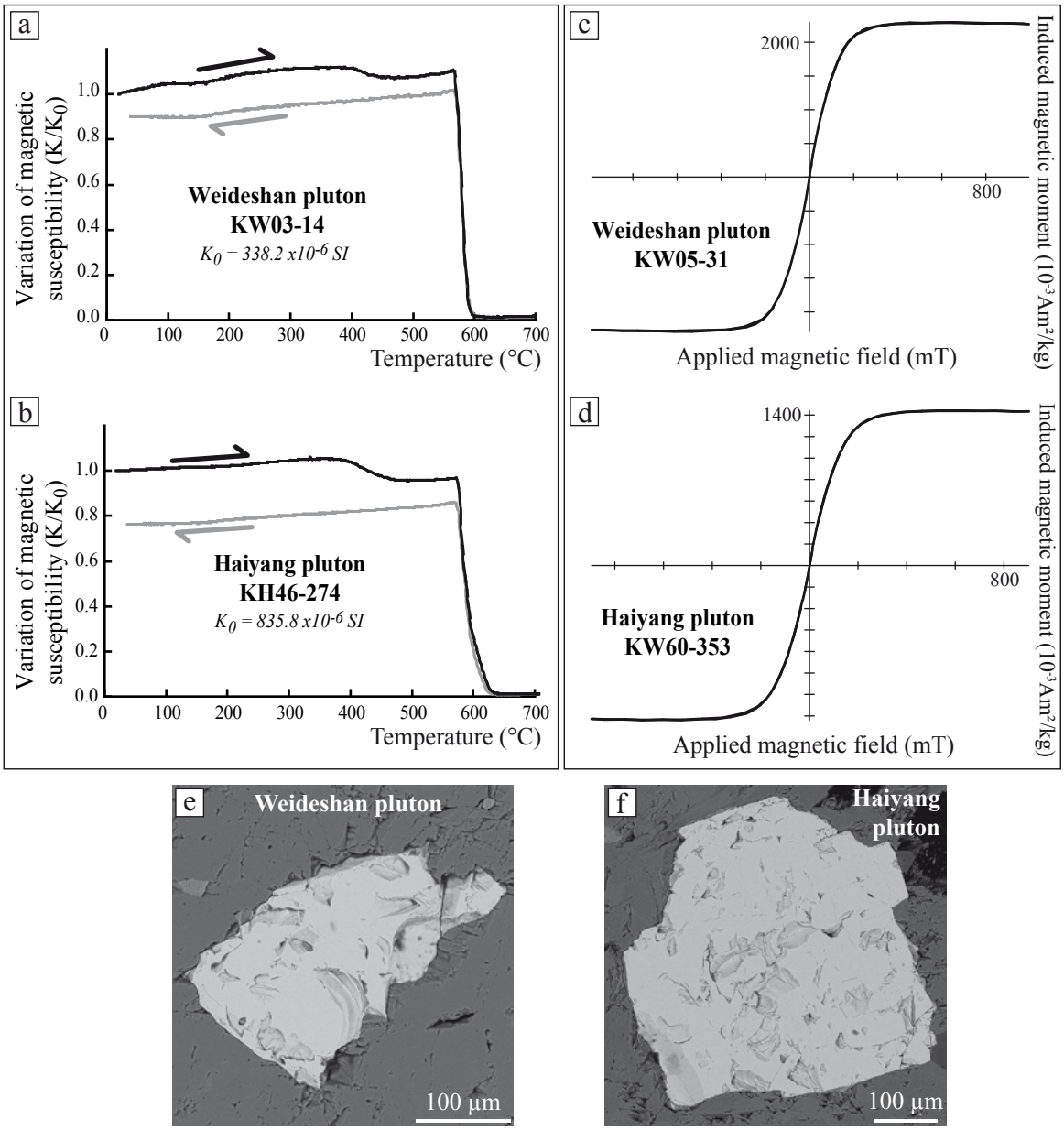
a
Variation of magnetic susceptibility (K/K0)
1.0
0.8
0.6
0.4
0.2
0.0
Weideshan pluton
KW03-14
K0 = 338.2 x10-6 SI
0
100
200
300
400
500
600
700
Temperature (°C)
b
Variation of magnetic susceptibility (K/K0)
1.0
0.8
0.6
0.4
0.2
0.0
Haiyang pluton
KH46-274
K0 = 835.8 x10-6 SI
0
100
200
300
400
500
600
700
Temperature (°C)
c
2000
800
Weideshan pluton
KW05-31
Applied magnetic field (mT)
Induced magnetic moment (10-3Am2/kg)
d
1400
800
Haiyang pluton
KW60-353
Applied magnetic field (mT)
Induced magnetic moment (10-3Am2/kg)

e
Weideshan pluton
100 µm

f
Haiyang pluton
100 µm

Figure 4

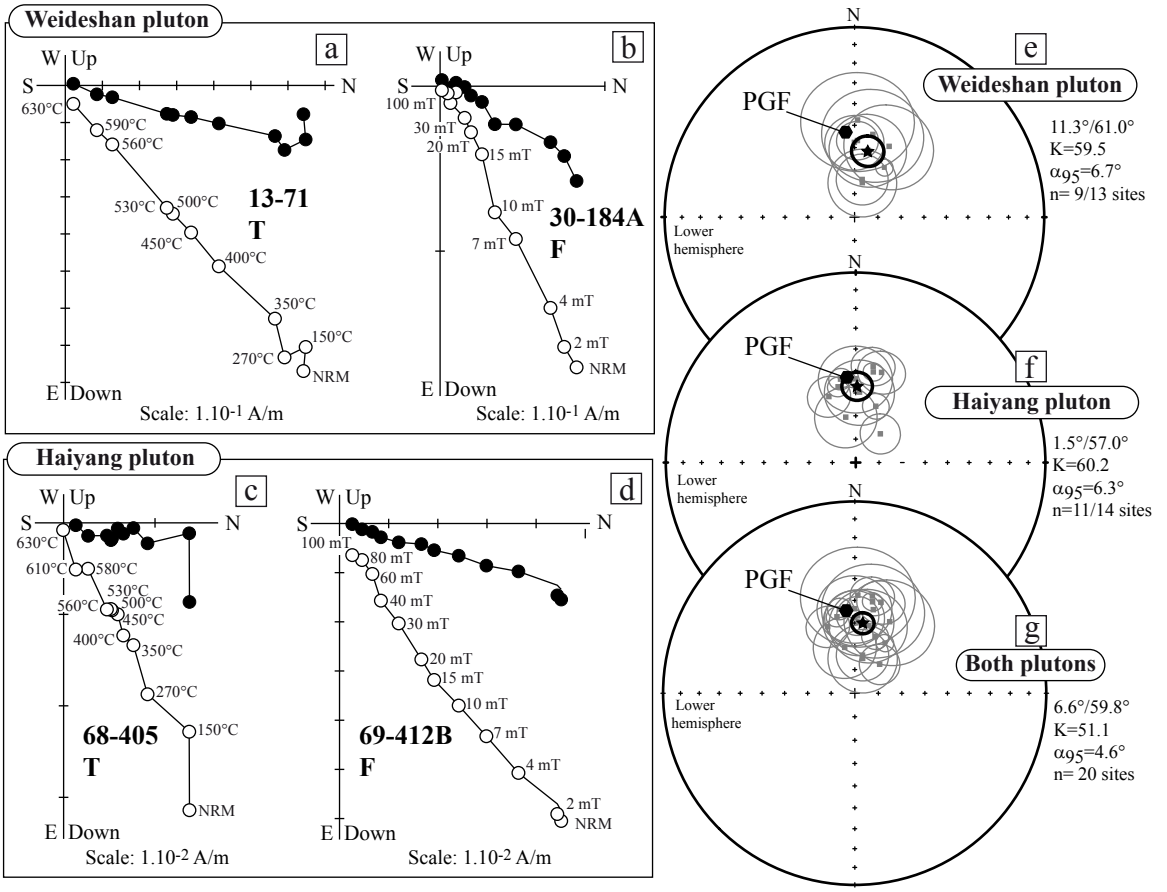
Weideshan pluton
a
W Up
S
N
630°C
590°C
560°C
530°C
500°C
450°C
400°C
350°C
270°C
150°C
NRM
13-71
T
E Down
Scale: 1.10-1 A/m
b
W Up
S
N
100 mT
30 mT
20 mT
15 mT
10 mT
7 mT
4 mT
2 mT
NRM
30-184A
F
E Down
Scale: 1.10-1 A/m
Haiyang pluton
c
W Up
S
N
630°C
610°C
580°C
560°C
530°C
500°C
450°C
400°C
350°C
270°C
150°C
NRM
68-405
T
E Down
Scale: 1.10-2 A/m
d
W Up
S
N
100 mT
80 mT
60 mT
40 mT
30 mT
20 mT
15 mT
10 mT
7 mT
4 mT
2 mT
NRM
69-412B
F
E Down
Scale: 1.10-2 A/m
N
e
Weideshan pluton
PGF
Lower hemisphere
11.3°/61.0°
K=59.5
α95=6.7°
n= 9/13 sites
N
f
Haiyang pluton
PGF
Lower hemisphere
1.5°/57.0°
K=60.2
α95=6.3°
n=11/14 sites
N
g
Both plutons
PGF
Lower hemisphere
6.6°/59.8°
K=51.1
α95=4.6°
n= 20 sites

Figure 5

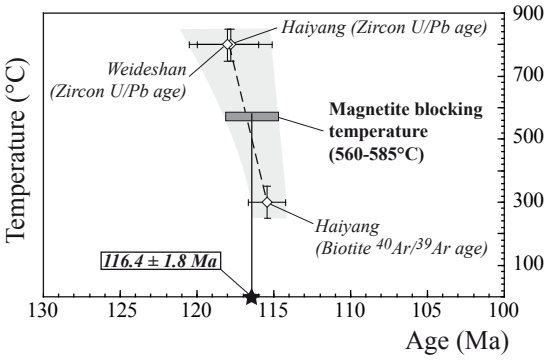
Haiyang (Zircon U/Pb age)
Weideshan
(Zircon U/Pb age)
Magnetite blocking
temperature
(560-585°C)
Haiyang
(Biotite 40Ar/39Ar age)
116.4 ± 1.8 Ma
Temperature (°C)
900
700
500
300
100
130
125
120
115
110
105
100
Age (Ma)

Figure 6

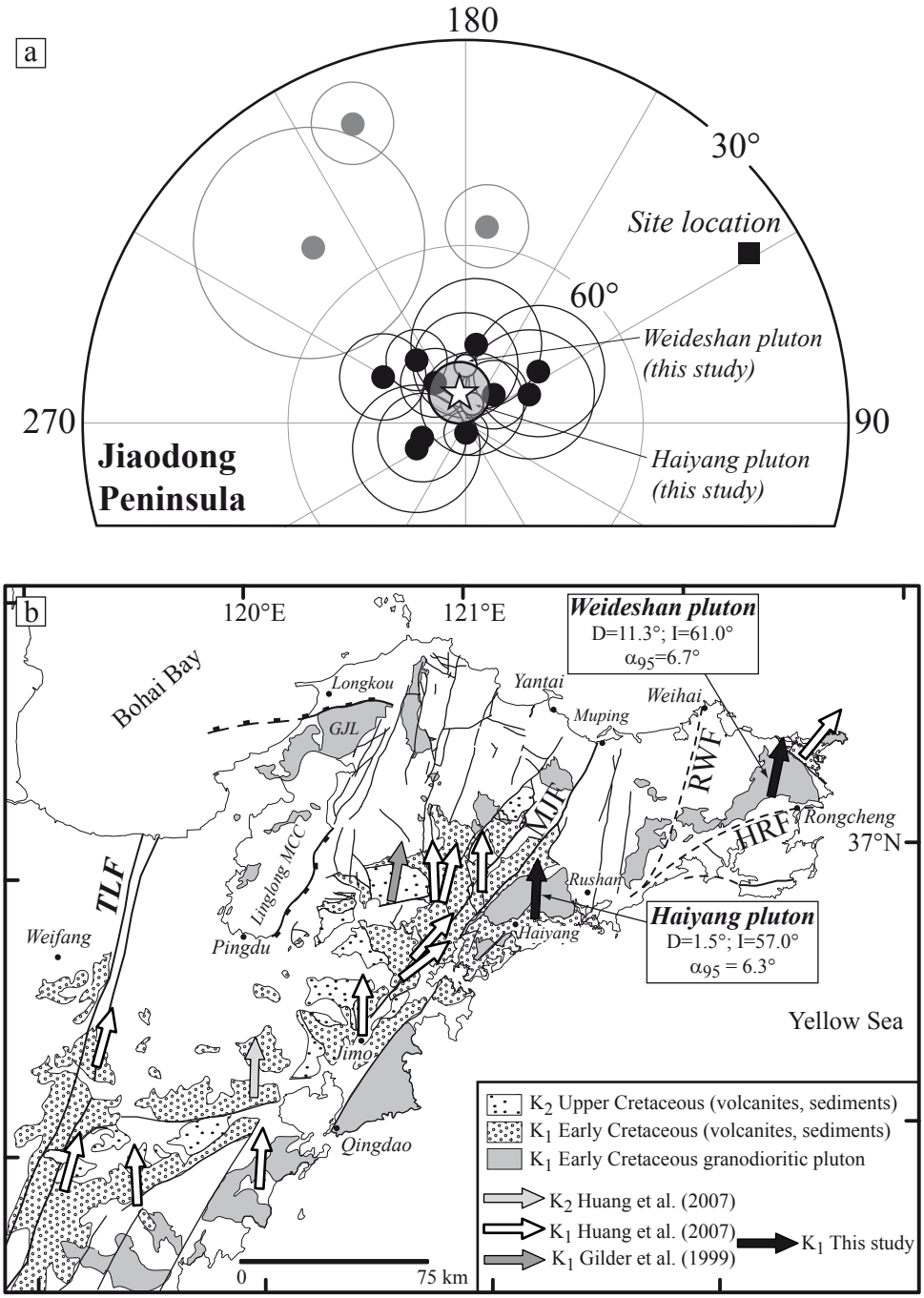
a
180
30°
Site location
60°
Weideshan pluton
(this study)
270
90
Jiaodong
Peninsula
Haiyang pluton
(this study)
b
120°E
121°E
Weideshan pluton
D=11.3°; I=61.0°
α95=6.7°
Bohai Bay
Longkou
Yantai
Weihai
Muping
GJL
RWF
MJF
HRF
Rongcheng
37°N
Linglong MCC
TLF
Rushan
Haiyang pluton
D=1.5°; I=57.0°
α95 = 6.3°
Weifang
Pingdu
Haiyang
Yellow Sea
Jimo
Qingdao
K2 Upper Cretaceous (volcanites, sediments)
K1 Early Cretaceous (volcanites, sediments)
K1 Early Cretaceous granodioritic pluton
K2 Huang et al. (2007)
K1 Huang et al. (2007)
K1 Gilder et al. (1999)
K1 This study
0
75 km

Figure 7

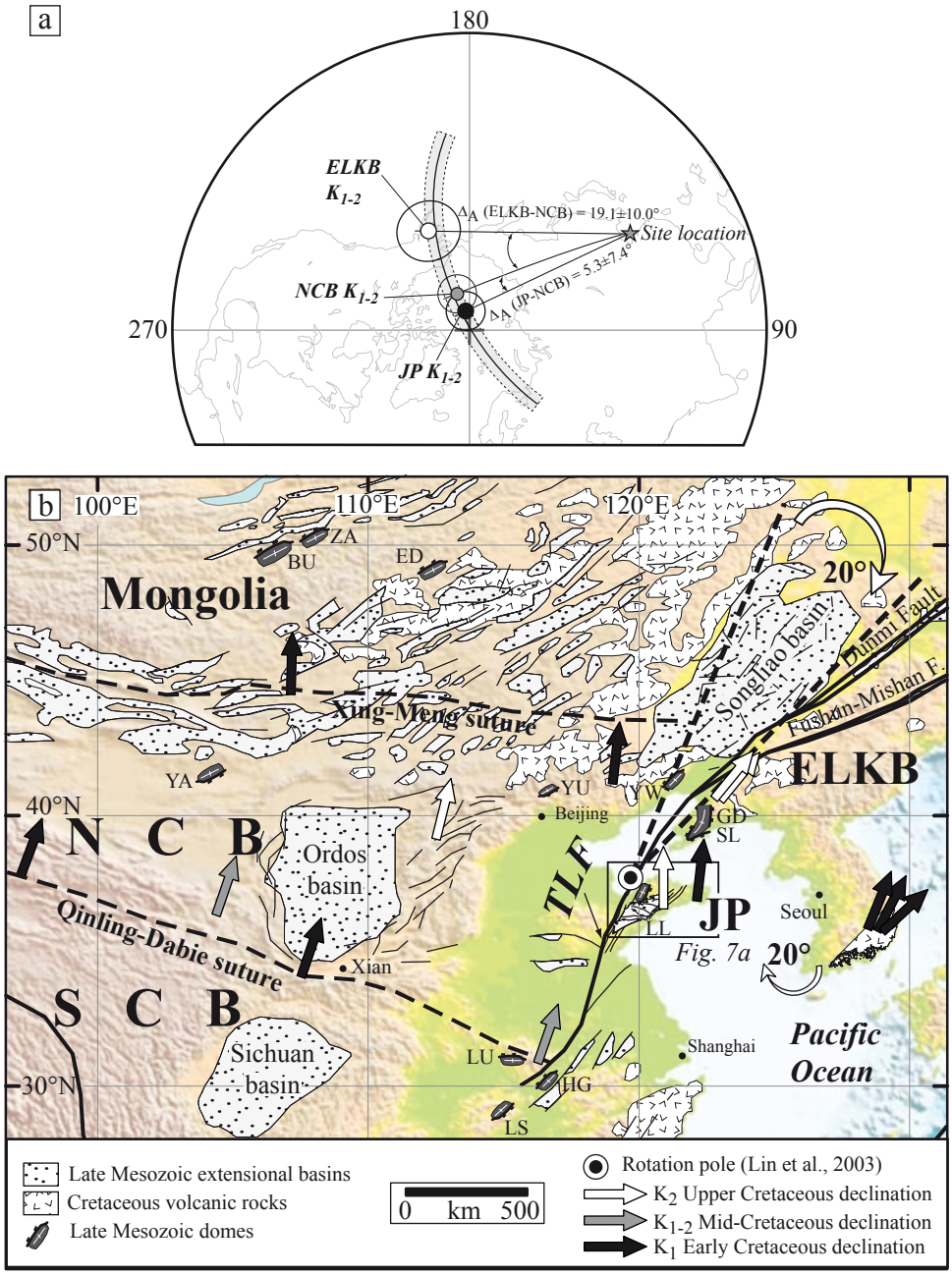
a
180
270
90
ELKB
K1-2
ΔA (ELKB-NCB) = 19.1±10.0°
Site location
NCB K1-2
ΔA (JP-NCB) = 5.3±7.4°
JP K1-2
b
100°E
110°E
120°E
50°N
40°N
30°N
Mongolia
ZA
BU
ED
20°
Songliao basin
Dunmi Fault
Fushun-Mishan F.
Xing-Meng suture
YA
YU
YW
ELKB
Beijing
GD
SL
N C B
Ordos basin
TLF
JP
Fig. 7a
LL
Seoul
20°
Qinling-Dabie suture
Xian
S C B
Sichuan basin
LU
Shanghai
Pacific Ocean
HG
LS
Late Mesozoic extensional basins
Cretaceous volcanic rocks
Late Mesozoic domes
0 km 500
Rotation pole (Lin et al., 2003)
K2 Upper Cretaceous declination
K1-2 Mid-Cretaceous declination
K1 Early Cretaceous declination

Figure 8

Site	Geographic coordinates		n/N	D	I	k	α_{95}
	Longitude (°E)	Latitude (°N)					
Weideshan pluton							
*KW01**	*122.420*	*37.200*	*0/6*			*excluded*	
KW10	122.410	37.230	4/4	11.3	60.5	33.6	16.1
KW13	122.384	37.273	5/5	31.0	65.1	435.1	3.7
*KW14***	*122.426*	*37.296*	*0/3*			*excluded*	
*KW17**	*122.440*	*37.340*	*0/4*			*excluded*	
KW20	122.340	37.250	5/6	359.9	57.7	40.1	12.2
KW23	122.275	37.287	5/5	2.2	56.8	79.3	8.6
KW30	122.330	37.230	3/3	12.6	53.2	35.8	20.9
KW32	122.462	37.246	4/6	1.8	47.6	17.1	22.8
KW36	122.501	37.294	3/5	26.1	55.9	44.3	18.7
*KW39**	*122.452*	*37.195*	*0/6*			*excluded*	
KW40	122.520	37.180	4/6	11.5	73.5	70.8	11.0
KW45	122.268	37.157	4/4	12.9	74.9	40.7	14.6
Mean			**9**	**11.3**	**61.0**	**59.5**	**6.7**
Haiyang pluton							
*KH50***	*121.170*	*36.850*	*0/5*			*excluded*	
KH54	121.130	36.870	6/6	337.9	59.3	56.5	9.0
*KH57***	*121.159*	*36.896*	*0/5*			*excluded*	
*KH58***	*121.140*	*36.890*	*0/5*			*excluded*	
KH60	121.140	36.890	4/6	16.1	49.1	90.3	9.7
KH67	121.076	36.834	5/6	19.7	64.3	188.8	5.6
KH68	121.212	36.837	4/5	3.1	59.6	41.2	14.5
KH69	121.290	36.870	5/5	11.0	49.8	344.2	4.1
KH70	121.267	36.893	5/5	359.8	53.7	26.7	15.1
KH74	121.220	36.930	4/6	10.3	47.3	110.0	8.8
KH281	121.379	36.911	6/6	40.7	73.8	61.7	8.6
KH286	121.369	36.858	3/5	346.9	56.4	804.1	4.4
KH290	121.360	36.809	5/6	347.7	70.1	34.3	13.2
KH294	121.301	36.832	6/6	349.7	53.2	196.2	4.8
Mean			**11**	**1.5**	**57.0**	**60.2**	**6.3**
Mean of both plutons			**20**	**6.6**	**59.8**	**51.1**	**4.6**

Table 1

Spots	U (ppm)	Th (ppm)	$^{232}Th/^{238}U$	^{206}Pb (ppm)	$^{207}Pb/^{235}U$	±1σ	$^{206}Pb/^{238}U$	±1σ	$^{207}Pb/^{206}Pb$	±1σ	$^{206}Pb/^{238}U$ Age (Ma) ±1σ
07-056/1	498.2	957.9	1.92278	41.4	0.12624	0.0021	0.01880	0.0004	0.04867	0.0005	120 ± 3
07-056/2	102.7	301.3	2.93445	8.8	0.12176	0.0036	0.01827	0.0004	0.04830	0.0006	117 ± 3
07-056/3	93.9	223.1	2.37640	8.8	0.13592	0.0044	0.01897	0.0005	0.05195	0.0008	121 ± 3
07-056/4	508.4	825.7	1.62414	51.3	0.15009	0.0027	0.01856	0.0004	0.05862	0.0006	119 ± 3
07-056/5	481.1	1457.8	3.03045	57.2	0.14080	0.0026	0.01852	0.0004	0.05513	0.0005	118 ± 3
07-056/6	370.2	1302.5	3.51842	44.5	0.14004	0.0028	0.01805	0.0004	0.05626	0.0005	115 ± 3
07-056/7	307.9	1676.5	5.44479	43.8	0.18468	0.0057	0.01908	0.0005	0.07020	0.0010	122 ± 3
07-056/8	315.5	1938.1	6.14211	44.0	0.12892	0.0076	0.01796	0.0006	0.05204	0.0017	115 ± 4

Table 2

Step	$^{40}Ar/^{39}Ar$	$^{38}Ar/^{39}Ar$	$^{37}Ar/^{39}Ar$	$^{36}Ar/^{39}Ar$	^{39}Ar	$\%^{39}Ar$	$\%^{40}Ar^*$	$^{40}Ar^*/^{39}K$	Age	Error
KH283				(e-3)	(e-14)				(Ma)	(1σ)
J= 0.00717										
1	9.233	0.054	0.00000	0.000	0.482	18.01	99.83	9.22	115.455	0.348
2	10.761	0.054	0.00000	6.003	0.089	21.35	83.37	8.97	112.474	2.930
3	9.589	0.054	0.00955	0.833	0.115	25.63	97.28	9.33	116.803	2.949
4	9.425	0.051	0.00612	0.000	0.092	29.09	99.83	9.41	117.787	1.001
5	9.425	0.051	0.00612	0.000	0.092	32.55	99.83	9.41	117.787	1.001
6	9.406	0.053	0.00000	0.000	0.144	37.91	99.83	9.39	117.551	0.670
7	9.321	0.054	0.00000	0.000	0.111	42.08	99.83	9.31	116.525	0.717
8	9.383	0.053	0.00063	0.000	0.290	52.92	99.83	9.37	117.272	0.500
9	9.281	0.052	0.00000	0.280	0.206	60.62	98.94	9.18	115.038	1.317
10	9.281	0.052	0.00000	0.280	0.206	68.32	98.94	9.18	115.038	1.317
11	9.462	0.054	0.00000	1.179	0.119	72.76	96.15	9.10	114.001	2.275
12	9.334	0.054	0.00056	0.945	0.165	78.93	96.84	9.04	113.291	1.641
13	9.080	0.051	0.00000	0.000	0.090	82.30	99.83	9.06	113.596	0.456
14	9.051	0.051	0.00000	0.000	0.090	85.68	99.83	9.04	113.245	0.454
15	9.193	0.052	0.00000	0.000	0.383	100.00	99.83	9.18	114.970	0.353

Table 3

Age		Slat (°N)	Slong(°E)	N	Plong (°E)	Plat(°N)	A_{95}	Reference
Jiaodong Peninsula (JP)								
K_1		35.97	119.15	4	172.3	76.4	11.1	Huang et al. (2007)
K_1		36.40	119.28	4	217.9	76.3	5.2	Huang et al. (2007)
K_1*		36.65	120.71	5	173.8	56.9	6.6	Huang et al. (2007)
K_1*		37.35	122.50	5	221.0	51.4	17.6	Huang et al. (2007)
K_1*		37.60	120.61	6	200.8	38.7	5.8	Huang et al. (2007)
K_1 (116 Ma)		37.27	122.41	9	180.1	80.1	9.0	This study (Weideshan)
K_1 (116 Ma)		36.89	121.29	11	161.1	86.5	8.9	This study (Haiyang)
K_1		35.90	119.45	6	114.1	78.0	11.0	Huang et al. (2007)
K_1		36.82	120.94	6	125.3	74.7	11.1	Huang et al. (2007)
K_1		36.97	120.86	3	240.9	73.8	7.3	Huang et al. (2007)
K_1		36.98	120.84	5	2.4	88.3	3.8	Huang et al. (2007)
K_1		36.00	120.00	20	135.0	83.1	5.9	Huang et al. (2007)
K_1		37.00	120.70	11	217.3	81.3	5.9	Gilder et al. (1999)
Mean K_1	JP			**10**	**177.1**	**83.0**	**5.5**	
K_2		37.00	121.00	4	297.5	80.5	10.9	Huang et al. (2007)
K_2		36.30	120.00	4	288.5	82.1	7.6	Huang et al. (2007)
Mean K_2		36.50	120.50	(8)	293.4	81.3	5.3	Huang et al. (2007)
Mean K_{1-2}	JP			**12**	**191.3**	**84.7**	**5.3**	
Eastern Liaoning-Korean Block (ELKB)								
K_1		35.90	128.50	19	205.1	67.6	5.8	Lee et al. (1987)
K_1		35.90	128.60	15	199.0	68.7	8.9	Zhao et al. (1999)
K_1		37.10	129.00	14	200.4	46.7	9.6	Doh and Piper (1994)
K_2		41.30	123.80	5	202.6	59.3	6.0	Uchimara et al. (1996)
K_2		41.30	123.80	7	205.5	59.4	7.3	Lin et al. (2003)
Mean K_{1-2}	ELKB			**5**	**202.4**	**60.4**	**8.5**	
North China Block (NCB)								
K_1		42.00	119.20	6	249.5	82.9	5.7	Zhao et al. (1990)
K_1		35.00	108.00	10	208.7	75.8	7.5	Ma et al. (1993)
K_1		45.40	107.60	3	247.6	87.3	21.6	Pruner (1992)
K_1		39.90	97.70	9	169.9	75.5	7.7	Chen et al. (2002)
Mean K_1	NCB			**4**	**204.0**	**81.7**	**9.2**	
K_{1-2}		37.20	105.00	10	203.4	74.5	8.2	Wu et al. (1993)
K_{1-2}		31.60	116.00	10	201.0	74.5	4.7	Gilder and Courtillot (1997)
K_2		40.10	112.90	4	170.1	79.6	5.8	Zheng et al. (1991)
Mean K_{1-2}	NCB			**7**	**198.7**	**79.5**	**5.2**	

Table 4